# POLITECNICO DI TORINO

**Master's Degree in Electronic Engineering**


Politecnico di Torino

**Master's Degree Thesis**

# Fiber optic based sensing systems for dynamic displacement and vibration monitoring


| Supervisors | Candidates |
|---|---|
| Prof. Guido PERRONE | Edoardo PANUELLO |
| Prof. Alberto VALLAN | Alessandro PICCARDO |


**October 2021**

# Summary

The main goal of this thesis is to develop a fiber optic sensor, more precisely a vibration sensor. The project consists on developing a working prototype using two different technologies, with two different optical circuits: the first uses two facing fibers, one in transmission and one in reflection, the second instead is based on a Bragg gratings, therefore the fiber is sensitive to contraction/expansion. The first arrangement is rawer and it is based on Plastic Optic Fibers (POF), it is cheaper and easier under both designing and manufacturing aspects. The second one, instead, exploits glass single mode fibers: it has a cost that is orders of magnitudes larger and requires a lot more effort to manage the optical components, because they must be fiber coupled.

Both optical circuits have as their output a light signal, which converges to a transimpedance and amplification circuit (signal conditioning), composed by 4 stages. The current provided by the photodiode carries the information about the sensed displacement inside its intensity and, since voltages are easier to manage, it has to be converted through a transamplifier. Then, two different inverting amplifiers are exploited to reach a suitable dynamics and, at the same time, to not saturate the OP-AMPs. The last stage is a buffer to increase the output impedance.

The output of this amplifier is read by an acquisition board based on ATMega328 architecture, which communicates through a PC. From what concern the communication between the microcontroller (the ADC board) and the calculator, two different types of communication have been implemented , serial and wireless. The first one relies on an USB wire that connects the sensor to the PC, while the second one exploits two radio modules working around 2.4 GHz. The receiving radio module is connected to the PC, where a Python multi process code is running. With the first process, the software is capable to catch all the transmitted samples, while the second one is used to generate a live plot that shows the past 500 samples, in order to monitor in real time the external perturbations affecting the sensor.

For this thesis the candidates have simulated, designed and assembled, entirely both optical circuits, designed and manufactured the PCBs, the design have been performed using a CAD software. For prototyping it has been decided to mill a PCB using a CNC machine, because it is more robust than a circuit on a breadboard and it will avoid some disturbances and parasitic capacitance. It has been programmed the microcontroller to sample the input signal and the protocols to connect with

the PC via serial and radio communication and developed a python software for the live plot of the sampled data. Furthermore, the system has been created and tested, confirming its functioning.

# Acknowledgements

Ai nostri amici, ai nostri colleghi, ai nostri compagni di merenda, a tutti coloro che si sono schiantati nella nostra vita lasciandoci un segno, grazie per essere stati nostri complici, per averci fatto crescere. Grazie alle nostre Mamme e ai nostri Papà, che nonostante la loro presenza silenziosa, sono sempre stati qui a sostenerci, a spronarci e ad aspettare di brindare ai nostri successi. Grazie ai nostri nonni, che hanno portato un pizzico di saggezza e affetto in questo percorso. Grazie a coloro che ci hanno fatto conoscere lo Spritz ed il San Simone, senza di voi non sarebbe stato così semplice studiare al Poli. Grazie ai nostri relatore e co-relatore, che oltre l' aiuto e la gentilezza mostrataci, si sono presi la briga di avere a che fare con questi due personaggi. Grazie a tutti coloro che hanno scelto di partecipare come parte integrante, nel bene o nel male, ad uno degli episodi più belli della nostra vita.
Infine vorrei ringraziare il mio compagno di tesi, nonchè caro amico, che mi ha aiutato ad affrontare con il sorriso, e con un goccio di beata ignoranza, il nostro ultimo saluto al Poli.

*A presto giovanotti*
*I vostri cari Ale ed Edo*

**Figure 1:** Ale ed Edo

# Table of Contents

# List of Figures

# Acronyms

**AI**
artificial intelligence

**MEMS**
Micro Electro-Mechanical Systems

**FBG**
Fiber Bragg Grating

**SMF**
Single Mode Fiber

**OSA**
Optical Spectrum Analyzer

**F-MZI**
fiber-optic Mach–Zehnder interferometer

**FDML**
Fourier domain mode-locked

**ISR**
Interrupt Service Routine

**SPI**
Serial Peripheral Interface

**AWG**
Arrayed Waveguide Grating

# Chapter 1

# Introduction

## 1.1 Context and problem statement

Nowadays, among the measurement systems for vibrations, the most developed, and sometimes even the cheapest, are the MEMS. The basic idea of a MEMS sensor is the creation of a mechanical structure that moves in some way according to the physical quantity to be detected. The mechanical structure is at the same time part of an electrical structure, for example a capacitor or a resistor. The variations of the physical quantity to be measured, in the study case, a vibration, cause the displacement of the mechanical structure, which slightly modifies the behavior of the electrical structure to which it belongs.

By detecting the tiny variations in the electrical behavior of the moving mechanical structure, an analog or digital output signal linked to the physical variable to be measured is obtained with appropriate processing. In MEMS vibration sensor the same thing is done, even if the dimensions involved are those typical of integrated circuits: the purpose of the micromechanical part of such device is to create a variable capacitor, whose capacity varies according to the applied displacement.

The level of effectiveness of MEMS sensors has reached an excellent level when they work in standard conditions, without having excessive stress due to the environment or due to the working conditions. Outside of certain ranges the device starts to give problems and the uncertainty about its measurements increases. As an extreme case it is also possible that it becomes dangerous, as, for example, at voltages above 50 V it is essential to adopt strict protection measures.

Other problems may arise due to the harshness of environment in which the sensor is placed: some of them may be, for example corrosion and electromagnetic disturbances. In conclusion there are conditions, in which MEMS fail to perform properly, such as in the environments mentioned above.

For these reasons, it is necessary to find a valid replacement that can take its place when the application foreseen for a MEMS vibration sensor does not allow it to function correctly. An alternative that is becoming increasingly popular is to use fiber

optic sensors, because they offer many and important advantages over traditional electrical sensors. Possible safety problems at work decrease drastically with optical fiber measurement technology: these sensors have no electrical conductivity.

## 1.2 Research objective

In recent years, an employment increase of fiber optics has been recorded in the sensors field. This growth can be explained by the fact that they have many better performances with respect to their electromechanical counterparts, while keeping a good quality and availability. Another important feature is that the same fiber can be used to collect data and to transmit them directly to a remote sink, for this reason this kind of sensors can be driven from a safe place, if the region under test is in a dangerous environment. Some other peculiar characteristics are: lightweight, resistance to corrosion, immunity to electrostatic discharges and impossibility to start fires.

Their main drawback is that the sensing device can be very cheap but interrogators needed to collect data from them can be quite expensive, so fiber optic setups are still only applied in niche application or when they are truly needed due to their particular features.

One of the main objectives of the research in this sector is to make sensor systems based on fiber optic technologies more affordable. In particular, the biggest obstacle to overcome is to be able to reduce the price of the device which, as mentioned, is often mainly due to data capture, rather than to the sensitive object itself.

## 1.3 Thesis contribution

The aim of this research is to study the feasibility of possible alternatives to traditional MEMS vibration sensors, using optical fiber-based technologies. During the elaboration two projects are carried out in parallel which differ in terms of the sensing principle used, while the acquisition part is the same for both.

The idea behind the first of these is to exploit the benefits brought by a measurement using Bragg grating, that is, by encoding the vibration in a wavelength variation. The big limitation of setup of this type is the interrogators costs, therefore it was decided to take advantage of a different and much cheaper approach called matched gratings, based on the comparison between two ideally identical optical fibers. The aim of this thesis is to demonstrate the effectiveness of measurement systems based on this method and evaluate their performances, in order to be able to compare them with different approaches for interrogating FBG.

With regard to the second approach, moreover, we wanted to take the concept of cost reduction to the extreme, producing a vibration sensor based on plastic optical fibers. This sensing method has a completely different approach and far worse measurement reliability, but, on the other hand, the cost for such a setup is

at least two orders of magnitude lower than the one previously described. Again, the purpose of this thesis is to show the pros and cons of this system in order to demonstrate its correct functioning.

Furthermore, the two types of systems have been compared with each other, in order to understand which are the applications for which it is better to use one, rather than the other.

Keeping the goal of limiting the price of the device as much as possible, an interface was also created that allows to view data from a PC. This was done by means of a simple and cheap microcontroller, so as not to be comparable with the price of the optical circuit and therefore not to ruin the cost performance. In this way the system obtains the shape of other commercial devices that also allow to see graphically the results of the measurements, transforming itself into a prototype that can be improved in order to put on the market a low cost alternative to existing products.

## 1.4 Thesis structure

The starting point of this thesis foresees the presentation of previous studies on the subject, in order to frame on the scale of technological development at what moment this work was produced. Furthermore, the state of the art is useful for providing a cognitive background regarding the topics that will be treated.

Subsequently, the software simulations that take into account the mathematical model will be presented, through which it was possible to carry out a feasibility study of the project. Furthermore, the results of these were used as a starting point for the design part of the hardware sensors.

After that, the thesis describes all the steps of concrete development, detailed of the reasons that led to the design choices of the entire hardware system: it starts from the optical vibration acquisition circuit, up to the analog conditioning circuit of the detected signal.

The next step is to explain how a microcontroller was programmed to acquire the vibration by transforming it into a binary value in order to be able to transmit it. To obtain the sampled data on the PC, as the thesis describes, it is necessary to create a communication between it and the microcontroller. This step has been implemented by means of both serial communication and radio communication. Both protocol programming processes are extensively discussed in the thesis. Finally, a python software is described which is in charge of collecting the data received on the PC, manage them and plotting them on the screen with a user interface.

The last chapter presents all the measurements made to verify the correct functioning of the system and compares the performance of the two different optic sensors at the base of the two arrangements studied.

# Chapter 2

# State of the art

## 2.1 Facing fibers sensor state of the art

The setup adopted in the studies is called 'Facing Fibers' and relies on the physical behavior explained below. The basic idea behind this kind of transducers is that a transmitting fiber emits a beam in free space toward a reflecting surface, then a second fiber is used as a receiver to collect the light coming back from the mirror. This beam is conveyed to a photodiode that transforms the light into a photocurrent, then it is converted in a voltage and acquired inside a proper interrogator. The distance can be measured starting from the amount of power captured after reflection: if the target surface is moving, the distance varies and so the power entering in the receiving fiber does. A sketch of how the system should look is presented in 2.1.

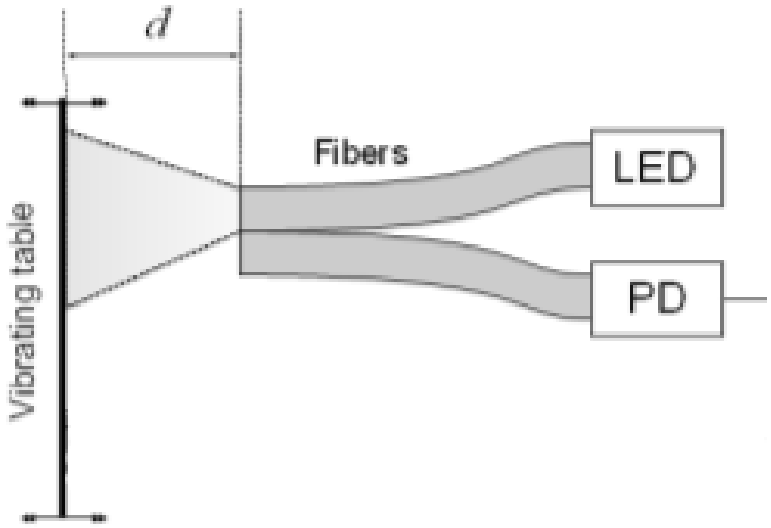


**Figure 2.1:** Facing Fibers setup

A very notable merit of this kind of arrangement is that the device is not in contact with the vibrating target, meaning that, if the device under test is very small (as, for example, micromechanics systems), the sensor can not affect its motion and inertia.

The main drawback, instead, is due to the fact that they are intensiometric transducers, so almost every component in the chain can lead to fluctuations in the output signal. Some kind of error sources can be, for instance: power level variations of the light source connected to the transmitting fiber, change in the target reflectivity (as aging, deposition of dirty, dust and other phenomena), geometrical parameters such as the uncertainty of the reference displacement, bending of the fiber, orientation of the sensing head and so on.

During the simulations, a second setup that requires a single fiber has been considered, it is based on the same idea of collecting the light coming back from a moving target after reflection. This kind of design is represented in Figure 2.2. The main difference with respect to the previous case is that, with this arrangement, both transmitting and receiving duties are assigned to a single fiber.

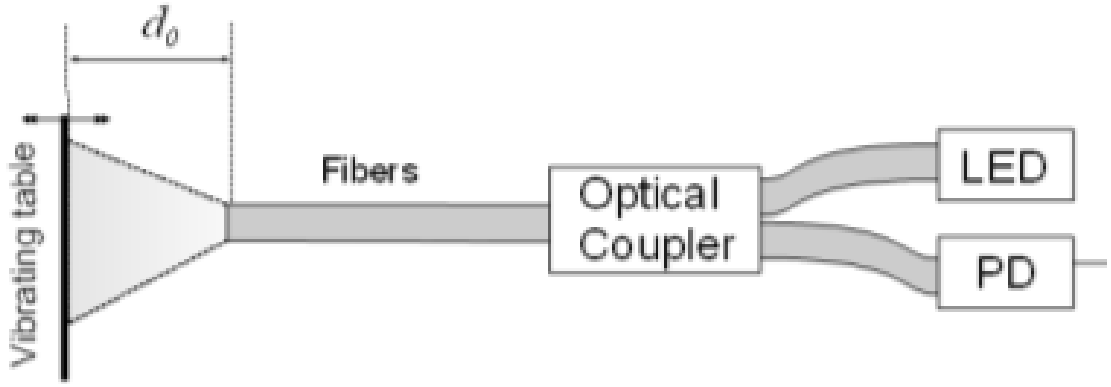


**Figure 2.2:** Single Fiber setup

With such configuration, the backward propagating wave is exploited to bring back the portion of collected light. Clearly, to avoid source damages and to get the resulting signal in an available end, it is required to place a circulator between the LED and the sensor fiber. In this way, the light can flow from the source (port 1) to the sensing lead (port 2), then the guided reflection propagates back on the backward wave to the circulator, it is transmitted from port 2 to port 3, where a photo-diode is connected. As for the facing fibers set up, the current exiting from it is the input of an interrogator that is able to perform some signal conditioning.

The main drawback of this kind of configuration is that the circulator brings an additional source of errors due to its non ideal directivity. More in the detail, this issue may not be so irrelevant for plastic optic circulators, since their behavior is quite poor because of the highly multimode conditions.

This kind of design for the sensing head has been studied only theoretically, simulations with different plastic fiber models are provided further in the discussion, but they have not been carried out experimentally to confirm the results obtained via software.

Furthermore, the two arrangements considered above have been merged to achieve the compensation of the target reflectivity: at least two received signal with different dependence from the target distance are required. The two can be, as just pointed out, the back reflection inside the transmitting fiber itself and the light captured by a receiving one. This method has been described in [1].

### 2.1.1 LED and photo-diode choices

Regarding the the light that has to be used in such applications, there is no need to have a single mode fiber, because it brings together all the coupling problems of that type of fiber. Furthermore, a SMF would require very expensive source and collector, because they should be able to transmit or collect only at the chosen frequency. Another arising problem would be that the incidence angle should be perfectly known and fixed, in order to let the optic fiber to guide correctly the mode inside its core. All these aspects would require an extra effort to precisely place of all the components, that are also not cheap. There are, so, two reasons to not exploit glass SMF in this kind of application.

A preferred alternative is to use cheap highly multimode POFs, that can guide up to millions of modes. In this way, even simple LEDs and photo-diodes are able to achieve the performances required. Another important improvement is that the POFs setup is not dependent on the incidence angle between the light and the fiber section: being extremely multimode, any orientation of the source leads to thousands of modes to be confined. So, using POFs, the mounting process can be simplified a lot and, at the same time, the setup cost is reduced by something around two orders of magnitude. Obtaining these huge benefits, all the drawbacks the POFs have with respect to single mode glass optic fibers are easily negligible: for this reason they have been exploited in the proposed application.

### 2.1.2 Different types of fiber bundles and their cross sections

About POFs, there exist several different fiber families, depending, as always, on the cross section: in particular on core and cladding diameter' sizes (the dependency of the application's behavior due to the fiber radius will be shown with more details in 3.1, where the support of numbers can corroborate the speech). Another exploitable option is to use bundles, that are composed of a common end to be connected to the light source from which branch off a variable number of tails. Using this kind of optic fibers, it is possible to exploit a single lead to transmit, while several others are in charge of collecting the reflected light. If several cores are used to receive the

mirrored light, the superimposing area is larger and so the captured power will. In this way it is possible to improve the sensitivity of the setup: considering N equal receiving cores, the collected light can increase up to N times the portion of light received by a single one.

[2] and [3] describe in a detailed way how to improve the performances of the sensor, by using different optical fiber bundles in place of a single optical fiber pair. Typically, the arrangement of optical fibers in the bundle front-end may be random (R), concentric (C), hemicircular (H), double circular (DC), concentric random (CR), concentric hemicircular (CH), or hemicircular random (HR), as shown in Figure 2.3.

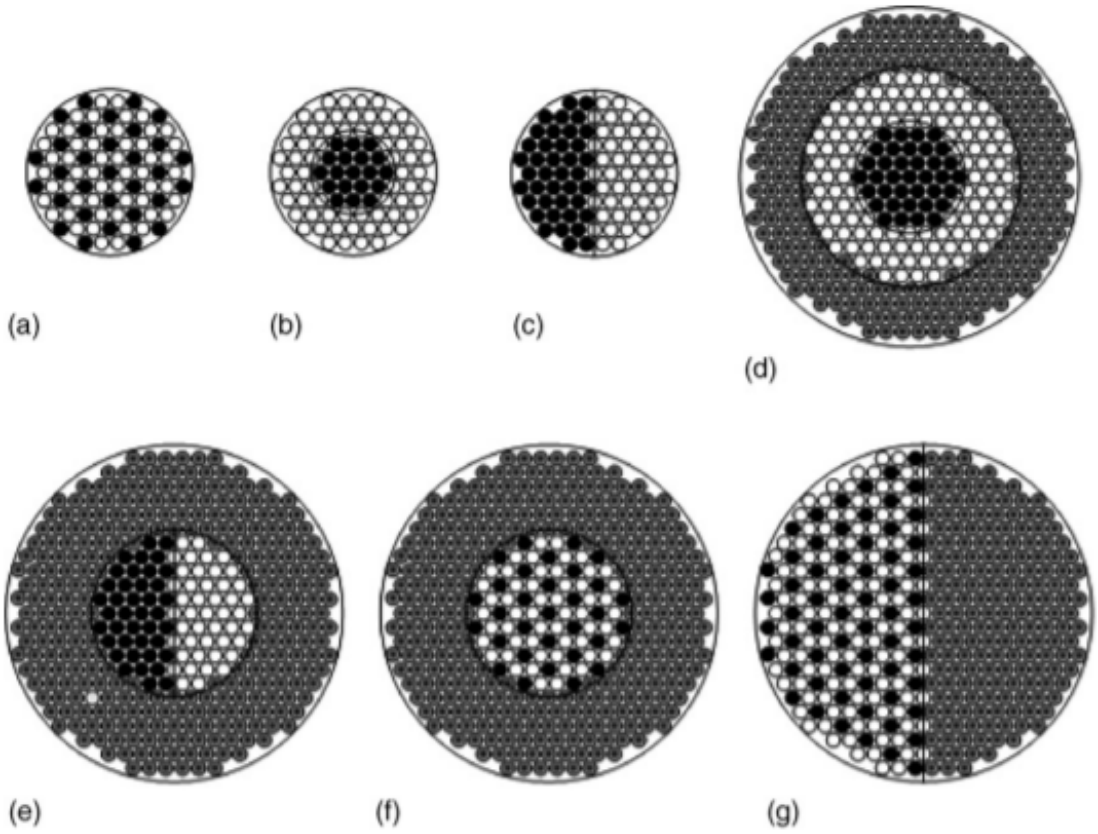


**Figure 2.3:** Bundle types

The main advantage of this kind of setup is, as said, the improvement of the sensitivity, since several receiving fibers are capable to collect more power. Furthermore, different transfer function and sensitivities are obtained by using different arrangements and this provides greater expandability and flexibility in the design of the sensor.

The disadvantage of using bundles, indeed, comes from the fact that it is a lot more difficult to describe a model true to the real sensor behavior. To solve this

drawback, the authors of [3] have developed and described theoretical models that may be applied to various bundle configurations. For a bundle with a small number of fibers, a summation model is explained there; while for a bundle with a large number of fibers, an integral model is proposed by introducing a parameter called the distribution density of the distance between fiber axes. Results are then compared by means of model and fiber bundle configuration used.

In [1], differently, the authors have used a Monte Carlo technique to analyze a POF bundle. Thanks to is type of investigation, it is possible to obtain a more realistic behavior of such arrangements, without having to consider a simplified ideal case of fibers facing perpendicularly a target with uniform reflectivity and with a Gaussian irradiance; these two are very strong and restrictive assumptions for POF bundles.

## 2.2 Fiber Bragg gratings state of the art

The advent of fiber-optic communication has revolutionized nearly all aspects of communication technology. In the past few decades, optical fiber sensors have been extensively researched and employed for various applications, such as measurement of strain, refractive index, vibration of structures and machines, electric current, voltage, impedance, temperature, pressure, humidity etc. The use of fiber Bragg grating, which alone can perform the basic function of reflection, dispersion, and filtering that can be easily utilized in sensing applications.

### 2.2.1 How fiber Bragg gratings work

FBG technology is one of the most admired choices of optical fiber sensors due to their simple manufacturing and relatively strong reflected signal. FBGs are formed by a periodic modulation of the index of refraction of the fiber core along the longitudinal direction. By grating, it is meant that there is a periodic change in the core's refractive index. When the light travels inside the grating structure, some portion of light gets reflected back from each grating plane. When the light travels inside the grating structure, some portion of light gets reflected back from each grating plane. Figure 2.4 shows the structure of simple fiber Bragg grating, every reflected portion of light combines to form one reflected beam of light, but this is possible only if Bragg condition is met. The Bragg condition is given by the following equation:

$$\lambda_{\mathrm{B}} = 2\Lambda n_{\mathrm{eff}}, \tag{2.1}$$

where $\Lambda$ is the grating period that forms the distance between two adjacent grating planes, $n_{\mathrm{eff}}$ is the effective core refractive index, and $\lambda_{\mathrm{B}}$ is the Bragg wavelength. When Bragg condition is met, all the reflected light constructively adds up to form backward reflected peak whose central wavelength is given by $\lambda_{\mathrm{B}}$.

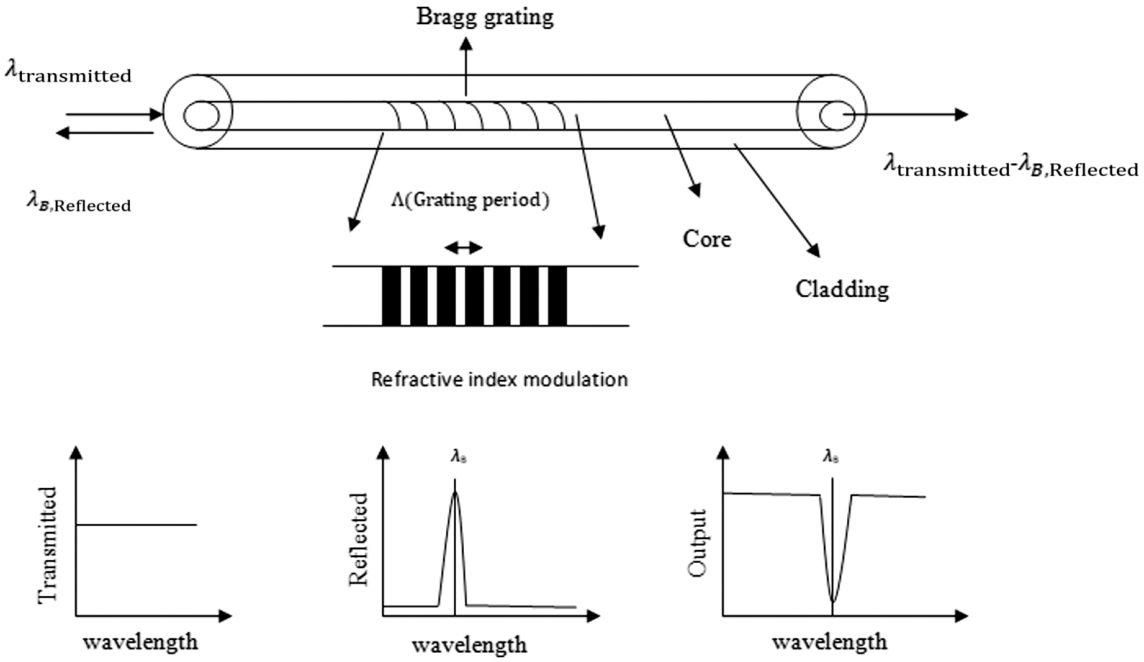


**Figure 2.4:** Structure of a fiber Bragg grating

### 2.2.2 How FBG are fabricated

Grating inside the fiber is formed using various methods. Broadly, there are two ways of writing, i.e., internal writing and external writing. Internal writing was first demonstrated by Hill using an argon ion laser and exposing the photosensitive fiber by coupling light in fiber core. The change in refractive index observed is very small therefore this type of writing is not useful. Externally inscribed writing is the most commonly used writing and can be performed with various ways, such as interferometer, phase mask technology, point-by-point technique, and line-by-line technique, but since there is an issue of change in wavelength of the laser in the case of phase mask technique, femtosecond pulse lasers are normally preferred, and this is the technique that has been used. Femtosecond pulsed laser technique provides fully customized grating. It involves formation of precise gratings using an ultrafast laser having time period in femtosecond. This technique uses different approaches to form gratings and can be achieved by the interferometric method, phase mask, point-by-point, line-by-line, and plane-by-plane inscription.

### 2.2.3 Sensing mechanism of FBG

An FBG sensor works on the principle of wavelength shift. Bragg wavelength depends on the physical parameters of the fiber, which are grating period and effective refractive index. Shift in the wavelength of reflected spectrum either to the left or right of central wavelength is caused only if either the period of gratings

or effective refractive index of FBG is changed by parameter to be measured, such as temperature, strain, humidity, pressure, etc. According to Bragg condition, wavelength change can be found, which is indicative of the amount of external perturbation applied on the FBG.

### 2.2.4 FBG-based strain sensors

Strain sensing is utilized in almost every type of industry and the most conventional method used is strain gauge technology for testing automobiles, infrastructures, etc. Due to inherent advantages of FBG, it has taken over conventional methods even though it cannot completely compete with strain gauges regarding price. But due to mentioned properties, they find a place in special applications involving modern constructions such as airplanes or wind power plant since they match quite well with composite materials employed in such areas. Fiber Bragg gratings for strain sensing play a very crucial role in almost every area of application, such as condition monitoring, structural health monitoring, and fault diagnosis. Stress applied on FBG induces change in either effective refractive index, which causes a change in wavelength shift. Strain sensitivity of FBG depends on physical characteristics of fiber such as thermo-optic coefficient and elasto-optic property and also on the type of strain (tensile or compressive) applied on it.

Strain gauge method for strain measurement is the most commonly used method where change in resistance due to induced strain is determined by Wheatstone bridge circuit. Since it is not electrically isolated, therefore it cannot be used in many applications where electrical isolation is necessary, so it is replaced with fiber optic sensors.

## 2.3 Bragg gratings sensor state of the art

The Fiber Bragg Grating is a diffraction grating inscribed in the core of a single mode fiber, which reflects a specific wavelength of the incident light, called the Bragg wavelength. The Bragg wavelength changes with the strain and temperature induced on the FBG. Due to the fact that they are instrinsically fire safety, they have electromagnetic immunity and high sensitivity, FBG sensors have been used in a variety of applications such as structural health monitoring, vibration sensing under high electromagnetic noise, for example in an industrial plant near some huge inductive motors.

Up to now there are some methods to measure FBG sensors, we can briefly classify them into three types:

- wavelength-swept filters
- interferometers
- passive filters or passive components

Firstly, the wavelength-swept-type interrogators employ a wavelength-swept light source or measurement window, the similar working principle of the OSA. The interferometer-type interrogators employ a kind of interferometer, such as Mach – Zehnder or Michelson ones. These have the great potential for measuring Bragg wavelength with extremely high precision and their methods have already been used in commercially available FBG interrogators, they will be presented later on in the details. However, these methods aren't so portable, and they are not proper cost effective. The last method is to develop a FBG interrogation system using some passive components, for example a photodiode, in order to convert a wavelength shift measurement, in an intensiometric one.

## 2.4 Interrogators state of the art

### 2.4.1 Fiber Bragg gratings interrogators

The key challenge in FBG sensing is the interrogation of the parameter where the signal is encoded in, the wavelength shift. The sensing principle of FBG sensors involves detection of central wavelength variation. Most conventional interrogation method utilizes an optical spectrum analyzer with broadband source as it performs direct measurement of the reflection spectrum of the FBG. However, OSA provides low resolution and slow response speed that cannot satisfy the requirements of accurately detecting the small and dynamic variations of the FBG's central wavelength. It can be used only for laboratory test purposes. Therefore, for real sensors, it is of significance to have interrogators that can work at high scanning speed to achieve dynamic sensing.

To demodulate the Bragg wavelength, a lot of methods, during these last years have been studied. There are various types of solutions to interrogate FBGs from the most expensive, for example using the optical spectrum analyzer, or more complex and sophisticated instrumentation (which will be discussed later on) to simpler but equally effective ways.

Methods such as interferometric technique, scanning filters, edge detection filter, wavelength-swept laser, and many more techniques can be used to measure such dynamic strain measurements.

#### Interferometric technique

An important FBG sensor interrogation scheme that has gained widespread acceptability is based on the principles of light interferometry. For example, an unbalanced fiber-optic Mach–Zehnder interferometer (F-MZI) is used as the wavelength discriminator. The interferometer converts the Bragg wavelength shift of the reflected light signal from the FBG sensor into a corresponding phase shift, which is finally recorded as intensity variations at the output of the F-MZI. This fiber-interferometric wavelength interrogation method has additional advantages of wide bandwidth, high

resolution, tunable sensitivity, etc., and is more suitable for dynamic measurement of strain as required in the fields of vibration and acoustics.

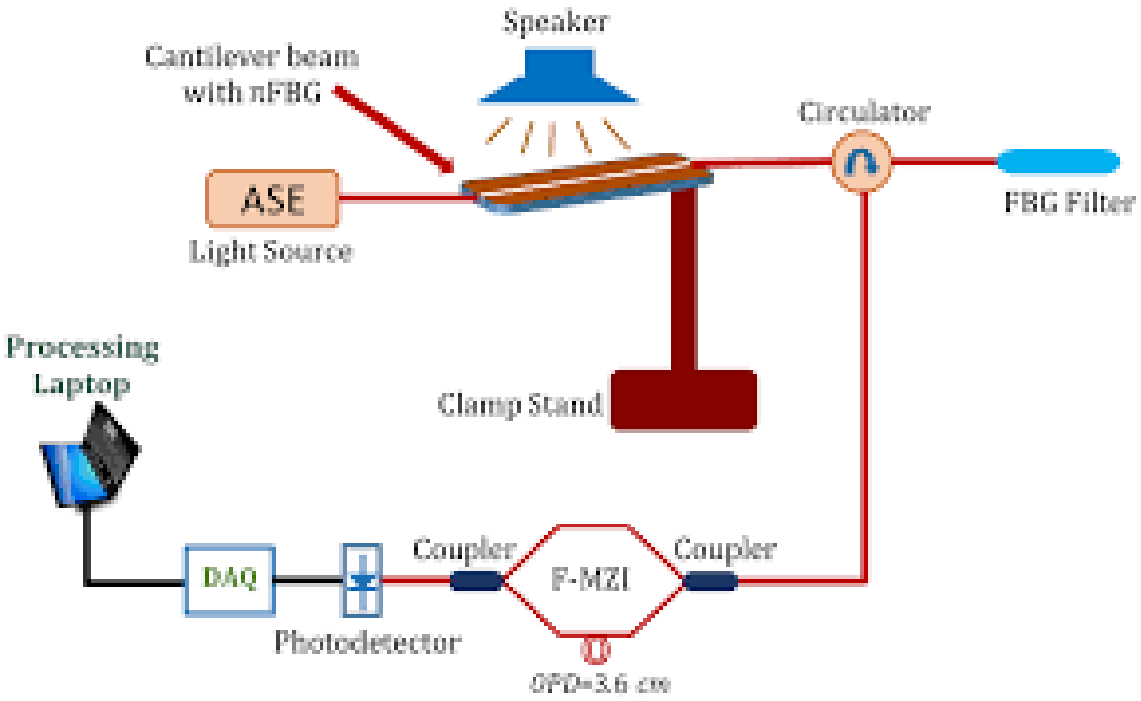


**Figure 2.5:** Fiber-MZI-based FBG sensor interrogation example

### Scanning filter based FBG interrogator

In this technique, light from an optical source is guided by fibers to the array of serially-multiplexed FBGs. Reflections from all FBGs are returned via a coupler to the interrogating device, at which the peak reflected wavelength from each sensor is extracted.

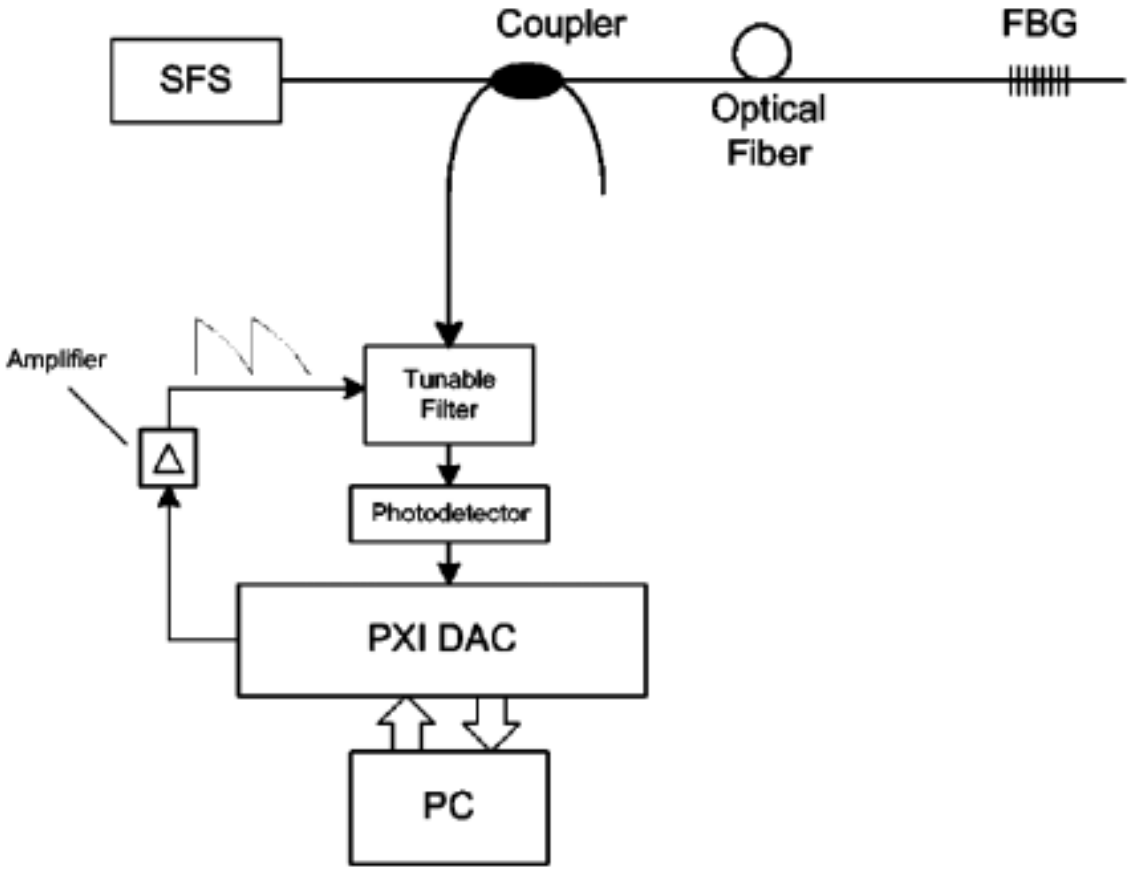


**Figure 2.6:** Scanning filter based FBG interrogator

In the above scheme (Figure 2.6), a tunable filter is scanned over the bandwidth of the source and the photodetector output is sampled continuously. Extraction and tracking of FBG peaks is performed usually by an appropriate software based on the recorded spectra.

### Optical edge filter technique

The use of an optical edge filter (Figure 2.7) can be considered to achieve a simple measurement setup. The optical edge filter is a kind of dielectric thin film, which is normally used as a WDM filter in a variety of applications such as telecommunications and sensor multiplexing.

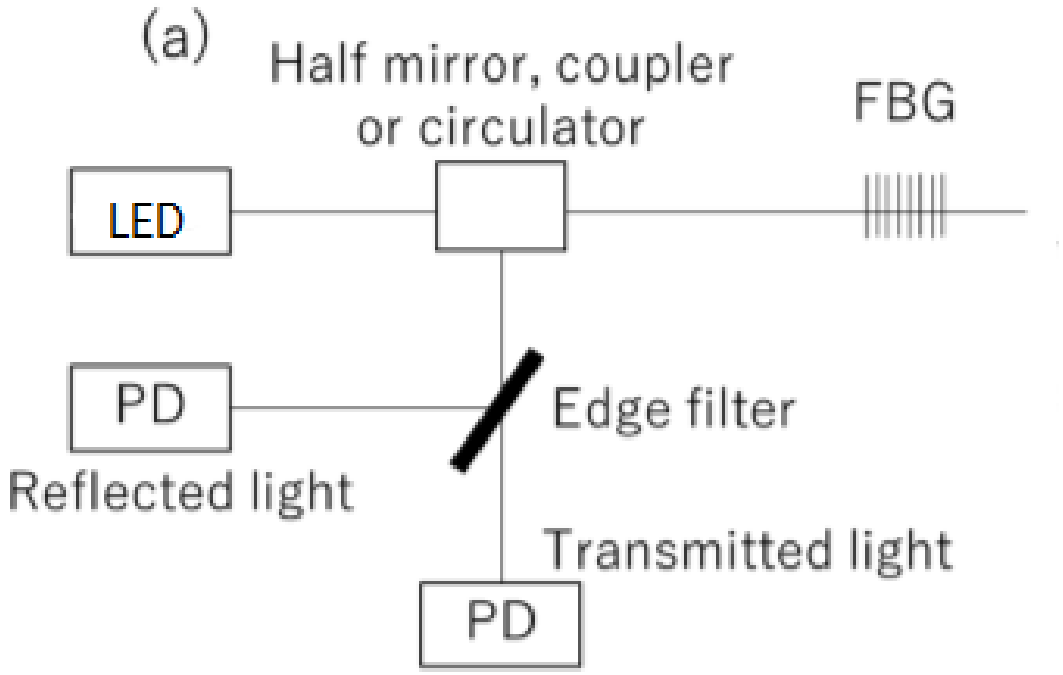


**Figure 2.7:** Edge filter

Methods such as interferometric methods, scanning filters, edge detection filter, wavelength-swept laser, and many more techniques can be used to measure such dynamic strain measurements.

### FDML wavelength swept laser

Figure 2.8 shows the schematic of a FBGs sensor interrogation system using the FDML wavelength swept laser.

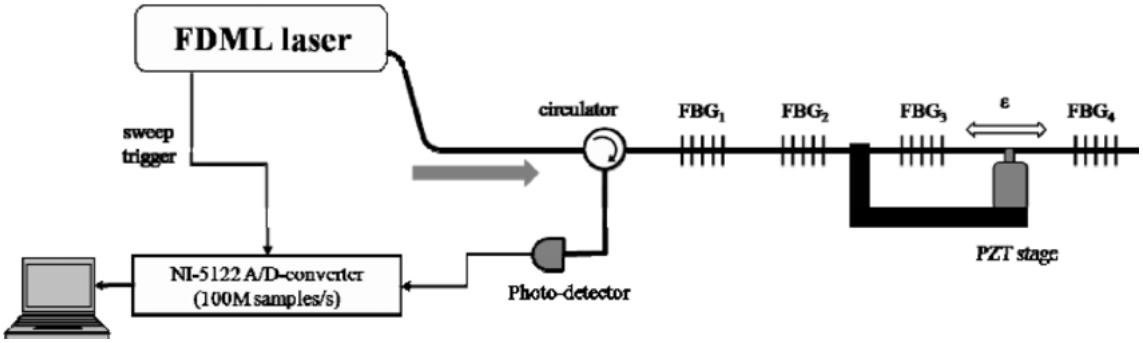


**Figure 2.8:** FDML wavelength swept laser interrogator

The laser output passes a circulator and is coupled into an array of four FBG sensors. By repeating the lasing peak scanning over the spectral range of the variuous FBGs sensors, it can simultaneously detect the reflected signals, which consist of a series of pulses in the time domain. Since the time intervals in the photo detector and spectral intervals of FBG sensors correspond to each other, the variance of the Bragg wavelength of each FBG sensors can be easily converted to the scanning speed of FDML wavelength swept laser source. In order to find the exact peak points in the time trace of the reflection signals, optimal algorithm program could be applied.

### 2.4.2 Matched gratings sensor technique

Since the classical interrogation methods of the Bragg gratings require particular and very expensive technologies (for example the optical spectrum analyzer (OSA), or the I-MON 256), one solution is to bring a noble quantity, therefore the displacement of a wavelength, in an intensiometric quantity. In order to do this, one of the most used techniques, which will be followed in this study, is the use of two matched gratings, and a photo-diode. Later on, in particular in chapter 4.2, it will be discussed with more details.

### 2.4.3 Interrogators instrumentation

#### OSA - Optical Spectrum Analyzer

The most practical and experimental way to analyze the fiber Bragg grating, is using the optical spectrum analyzer. Among the numerous advantages, the resolution bandwidth and the easily configurable SPAN must certainly be considered. Furthermore, considering to be able to connect a management interface including an acquisition card (in the studied case Keysight PCIB connection expert), it makes the instrument very versatile, giving the possibility to subsequently analyze the sampled spectrum. Unfortunately, the optical spectrum analyzer, in addition to being very cumbersome, is very delicate and expensive, this leads to consider new techniques and new approaches. Figure 2.9, shows a standard analysis setup for measuring the spectrum of an FBG.

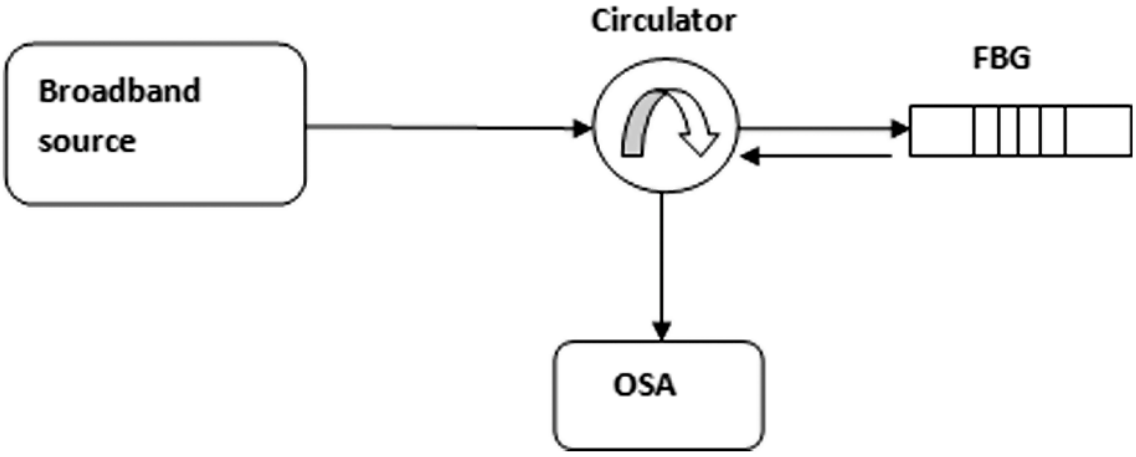


**Figure 2.9:** Interrogation of FBG using OSA

### si155 - HYPERION Optical Sensing Instrument

Luna's Micron Optics HYPERION si155 is an industrial grade fan-less optical sensing interrogator. It has 4 parallel channels of 160 nm on which it can perform static and dynamic spectrum acquisition, each one can be reached from the outside through an LC/APC optical connector. To connect the interrogator to the PC, instead, an Ethernet cable is exploited. The measurement system of the si155 features an ultra-wide swept wavelength laser realized with Micron Optics patented Fiber Fabry-Perot filter and wavelength reference technology. Furthermore, a DSP and an FPGA are integrated on board to perform data processing, so that also a peak detect function is implemented with low latency for closed loop feedback applications, other than the full spectrum acquisition.

**Figure 2.10:** si155 interrogator

Each channel has equal working capabilities, performances only depend on the chosen measurement option, out of the three available: Enhanced visibility (10 Hz), Standard (100 Hz or 1,000 Hz) or High speed (5,000 Hz). In particular the figure of merit changing are: wavelength accuracy, stability and repeatability, continuous and dynamic range.

The sensor types supported by this interrogator are: Fiber Bragg Gratings, Long Period Gratings, Fabry-Perot and Mach-Zehnder Interferometers.

More details about the si155 - HYPERION Optical Sensing Instrument can be found in [4], while Figure 2.10 shows how this device looks.

### I-MON 256 USB / 512 USB

The I-MON 256/512 USB can monitor in real-time a spectrum coming from an FBG sensor, the device is shown in Figure 2.11. Thanks to the USB interface, it is possible to get spectra with an acquisition up to 6 kHz (with the I-MON 256 USB) and 3 kHz (with the I-MON 512 USB), while keeping the resolution below 1 pm. Connecting the I-MON to a PC, it is possible to exploit thee software to develop measurement applications.

The working principle is based on a spectrometer technology that uses fused silica transmission gratings. The device is capable to split its spectrum in order to do parallel processing on several FBG sensors, whose peaks are measured by a diode array.

Comparing the datasheet of this device with the si155 manufactured by Micron Optics, it is possible to notice that it has a better resolution ($<0.5$ pm against $>1$ pm), but the wavelength range is smaller. Furthermore, the largest measurement frequency of the I-MON (6 kHz) is higher than all the three working speeds of the si155 (fastest

is 5 kHz). In terms of dynamic range, the better device depends on the sapling speed adopted: at lower frequencies si155 has a better response, while at higher ones it has worse performances. For more comparison details, datasheets are reported in [4] and [5].

**Figure 2.11:** I-MON 256 USB / 512 USB interrogator

### 2.4.4 Facing fibers interrogators

As for FBG method, also for facing fibers setup there already exist some commercial products able to interrogate the optic sensor. Interrogators of this kind are much cheaper than the ones in charge of measuring the Bragg wavelength shift, as widely pointed out in the previous sections.

More into the detail, [6] is the datasheet of a device that could possibly be used for the purpose. In reality, it is thought as a fiber optical accelerometer, but, by simply reading the description given on the datasheet, it is clear that, except from the sensor application, this device does exactly what it is required to interrogate the facing fiber version of a vibrating optic sensor. All features and characteristic parameters of this instrument can be found in [6].

# Chapter 3

# Simulations

## 3.1 Facing fibers simulation

The simulation of the POF system behavior has been carried out following the mathematical model described in [7]. The equations have been rearranged to the study case and implemented on a MATLab code so that it is possible to get the power collecting capability with respect to the distance from the mirror. The output is given graphically and it is computed for both the facing fibers and the single fiber methods. In facing fibers simulations, the transmitting and receiving leads are assumed to be equal, i.e. with same geometrical parameters (as core radius, cladding radius and numerical aperture), this is a fair assumption, as also in the concrete development they will. Since the work is carried out with largely multi-mode POFs, the modes carrying guided power along the fiber are so many that it is almost impossible to have dark spots on the circular cross section at the transmitting end. For this reason, it is preferred to not use the Gaussian approach explained in [7], since it accounts the total beam as the superposition of all the single mode Gaussian beams. Exploiting this method leads to have the light from the TX fiber to be described not by a ray cone with sharp boundaries, but by a non constant irradiance (or intensity) over the beam cross section: it decreases radially obeying to an exponential law. In place, the simulation has been fulfilled with the other approach described in the article, the geometrical one. With this method, the total beam is treated as a step of irradiance, meaning that all the points inside the cross section and with same propagation coordinate will all get the same value, while to the ones outside the circle is assigned a value of zero, as equation 3.1 shows.

$$\begin{cases} I(z) = \frac{P_e}{\pi\omega^2(z)}, \text{ inside the cone} \\ I(z) = 0, \text{ outside the cone} \end{cases} \tag{3.1}$$

### 3.1.1 Facing fibers simulation

Regarding the receiving end, what said before is still valid, so it can collect whatever reaches its cross section without giving rise to problems regarding the angle of incidence.

In the code, firstly, the following fiber parameters are defined:

- Core radius: $r_{\mathrm{co}},$ [µm];
- Cladding radius: $r_{\mathrm{cl}},$ [µm];
- Numerical aperture: $NA$;
- Direction of propagation coordinate array: $z,$ [µm];
- Radial coordinate array: $r,$ [µm];

The only dependencies on the physical realization of the POF are linked to the first three items of the list above, meaning that it is very easy to switch from a fiber simulation to another: it is enough to modify their values inside the declarations. The two arrays represent the two coordinates relevant for the case, that are the beam direction of propagation and the radius of the light cone (since it is considered a perfectly circular cross section, only a coordinate is enough to discriminate the points inside and outside the circle).

The above assumption lets it treat the light exiting from the transmitting fiber as a perfectly symmetrical cone with divergence angle $\theta_{\mathrm{a}}$ and vertex located at a distance $z_{\mathrm{a}}$ inside the bundle.

Then, knowing the geometry of the two fibers, it is possible to derive some fundamental parameters with the equations below:

- Spacing between the RX and TX fibers center: $d_{\mathrm{min}} = 2\, r_{\mathrm{cl}},$ [µm];
- Displacement between the center of the transmitting fiber and the beginning of the RX fiber core, i.e. the place where the RX end becomes sensitive: $displ_1 = 2\, r_{\mathrm{cl}} - r_{\mathrm{co}},$ [µm];
- Displacement between the center of the transmitting fiber and the end of the RX fiber core, i.e. the place where the RX end becomes insensitive again: $displ_2 = 2\, r_{\mathrm{cl}} + r_{\mathrm{co}},$ [µm];
- Divergence angle: $\theta_{\mathrm{a}} = \sin NA,$ [rad]
- Cone vertex: $z_{\mathrm{a}} = r_{\mathrm{co}}\ \cot\theta_{\mathrm{a}},$ [µm]
- Distance from the reflecting target: $h = (z - z_{\mathrm{a}})/2,$ [µm]
- Circular cross section radius: $w = z\ \tan\theta_{\mathrm{a}},$ [µm]

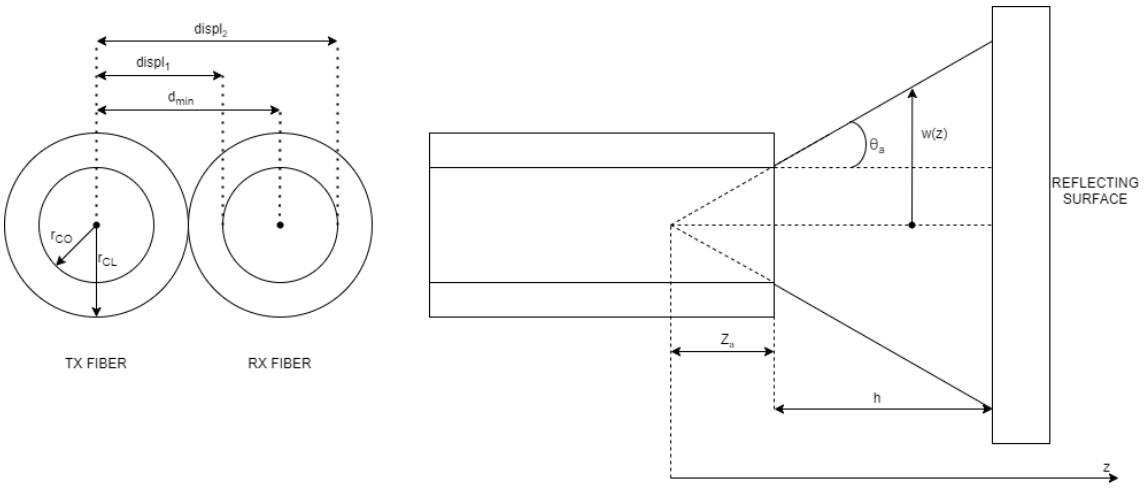


**Figure 3.1:** Fiber displacement parameters

In figure 3.1 it is shown what they are representing. In the geometrical passages below, they will be very useful to be defined in this way. It is already appreciable how a minimum distance between TX/RX fibers and the reflecting surface is needed, since the displacement $d_{\min}$ brings an insensitive region caused by the fact that the core is the only part of the fiber that can transmit or receive. This dead end could be removed only by removing all the layers above the two cores and placing them in contact, one next to the other. In reality, this is clearly not possible, but it is not a real issue because it is better to avoid such small distances from the mirror. The reason behind this sentence comes from the fact that a very large displacement of the mirror can make it touch the optic side, ending up damaging the components or moving them from their desired position.

Considering the reflecting surface as a planar mirror, an important conceptual simplification is to virtually extend the light cone beyond the mirror, so that the RX bundle mirrored image is met at double the real propagation length. This is the reason of the division by 2 inside the equation that gives the distance from the target.

Simple trigonometry can be applied to calculate the radius of the cross section as a function of the distance z travelled along the propagating coordinate.

As already pointed out before, the light intensity is assumed constant inside the cone and null outside, equation 3.1 explains how it is computed to clear its dependency on the distance z covered.

A qualitative approach tells that, after the insensitive region, the collected power should begin to grow due to the fact that the cone cross section starts to overlap with the receiving bundle core. In the range where the overlapping area increases progressively, it can be expected that the collected power should grow monotonically. Then, after the receiving core is fully illuminated, the collected power should start to decrease, since the overlapping area is now constant and, going further from the

source, the power density reduces, due to the fact that the light beam enlarges.

The next step is to define the three regions just mentioned: to do this, two pointers have been exploited, with which it is possible to divide the propagation axis $z$. The first one defines in the vector index where the beam radius $w = displ_1$, that is where the overlapping region starts. The second one, indeed, is used to describe the sector in which the superimposition of the two circles is variable, so $displ_1 < w < displ_2$. These indexes are useful to compute the overlapping area, that is a fundamental parameter for the received power calculation. In particular, it is clear that in the first region $Area = 0$, as explained above; on the contrary, in second and third sectors this sufrace must be computed.

The computation of the area in the region with variable overlap follows the passages present in the appendix of [7], described in Figure 3.2 and in the equations below.

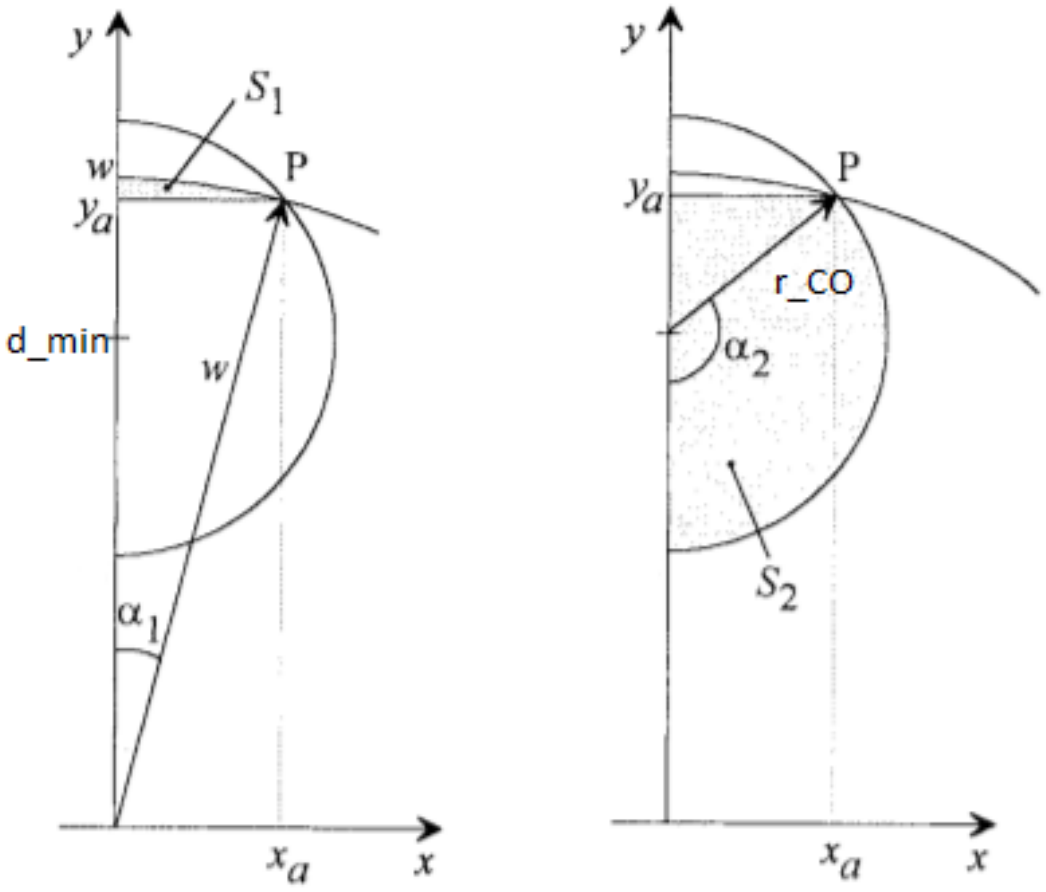


**Figure 3.2:** Geometrical separation of the Area

The angles $\alpha_1$ and $\alpha_2$ represented in picture are described in a different way with

respect to the article, as in 3.2 and 3.3:

$$\alpha_1(z) = \arccos \frac{d_{\min}^2 + w^2 - r_{\text{co}}^2}{2 d_{\min} w} \tag{3.2}$$

$$\alpha_2(z) = \arccos \frac{d_{\min}^2 + r_{\text{co}}^2 - w^2}{2 d_{\min} r_{\text{co}}} \tag{3.3}$$

Knowing the angle $\alpha_1$, through equations 3.4 and 3.5, the coordinates of the point P are found thanks to trigonometry.

$$x_{\text{a}} = w \sin \alpha_1 \tag{3.4}$$

$$y_{\text{a}} = w \cos \alpha_1 \tag{3.5}$$

Since the overlapping area is symmetrical, it is possible to compute the two regions shown in Figure 3.2, $S_1$ and $S_2$, and obtain the total as $S(z) = 2(S_1(z) + S_2(z))$. The two partial values are calculated as follow( equations 3.6 and 3.7).

$$S_1(z) = \frac{1}{2}\alpha_1 w^2 - \frac{1}{2} x_{\text{a}} y_{\text{a}} \tag{3.6}$$

$$S_2(z) = \frac{1}{2}\alpha_2 w_{\text{a}}^2 + \frac{1}{2} x_{\text{a}} (y_{\text{a}} - 2 w_{\text{a}}) \tag{3.7}$$

Finally, the power collected in the region $displ_1 < w < displ_2$ can be calculated as the product of the collecting surface $S(z)$ times the irradiance $I(z)$, as in equation 3.8.

$$P(z) = \frac{P_{\text{e}}}{\pi \omega^2(z)} S(z) \tag{3.8}$$

In the section where $w > displ_2$, the collected power is computed in a similar way, with the only difference of a constant overlapping surface equal to the the receiving core area: equation 3.9 shows the procedure.

$$P(z) = \frac{P_{\text{e}}}{\omega^2(z)} r_{\text{co}}^2 \tag{3.9}$$

Summarising, the power collected as a function of the distance between the fibers and the target is described by the following system (3.10):

$$\begin{cases} P(z) = 0, \ w < \text{displ}_1 \\ P(z) = \frac{P_{\text{e}}}{\pi \omega^2(z)} S(z), \ \text{displ}_1 < w < \text{displ}_2 \\ P(z) = \frac{P_{\text{e}}}{\omega^2(z)} r_{\text{co}}^2, \ w > \text{displ}_2 \end{cases} \tag{3.10}$$

Plotting the results obtained by the equation system above, the output produced are reported in Figure 3.3 and Figure 3.4. The first one shows the behavior of the

normalized power, that is transmitted over received, against the distance, while the second one is representing the sensitivity of it: it has just been computed as the derivative of it over the propagation coordinate.

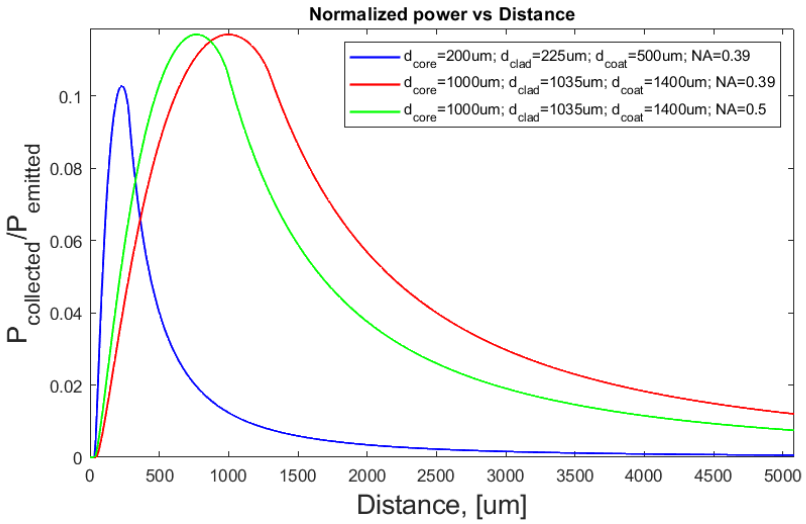


**Figure 3.3:** Normalized power of three different POFs

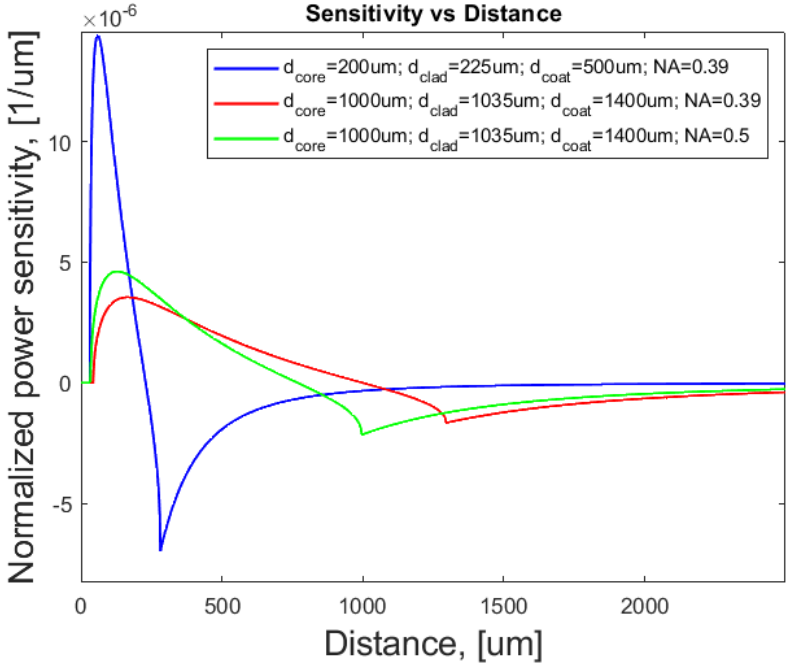


**Figure 3.4:** Sensitivity of three different POFs

On the figures, three different simulations have been performed: the curves

represent three plastic optic fibers differing on numerical aperture and cross section sizes. As expected, by increasing the core diameter, the capturing capabilities slightly increase and, reasoning in geometrical terms, the complete illumination of the receiving fiber occurs at a further distance from the mirror, since the cross section has more area to be covered by the diverging beam. Another feature to notice is that, comparing the two fibers with equal cross section, their simulations lead to the same peak intensity, but larger numerical apertures lead to nearer peaks: this means that, as confirmed by the second graph, the sensitivity is slightly better using the plastic optic fiber represented in green, so the one with $NA = 0.5$.

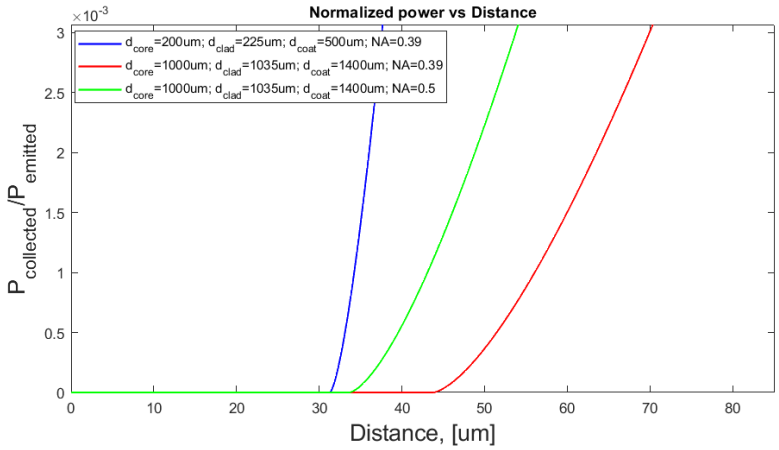


**Figure 3.5:** Zoom in of the normalized power graph

Furthermore, as appreciable from the zoom in of Figure 3.5, around the zero distance from the target surface, it can be noticed what previously said: there is a dead end zone where the sensor is not capable to capture the distance from the screen. This region is absolutely to avoid, because there the system would be completely insensitive to strains and contractions, but, fortunately, it is a quite small area. Another reason to avoid such small distances has already been presented, it comes from the fact that placing the two fibers so near the mirror can lead to troubles in case of very strong unexpected vibrations, that would make the two components touch. As a last consideration on these two plots, it can be noticed that the region where the device is not able to sense enlarges if the coating diameter increases: this is due to the fact that it leads to a larger distance between the transmitting core and the beginning of the sensible region of the receiving one. Analyzing the two fibers with equal diameters, instead, it can be seen how the numerical aperture affects the dark region: if NA is larger, the beam has a greater divergence, so the light can cover the displacement caused by the fibers in less space along the propagating axis.

Having performed all these considerations about the three simulated fibers, it is clear that the best performances are given by the one with $d_{\text{core}} = 1{,}000\,\mu\text{m}$, $d_{\text{clad}} = 1{,}035\,\mu\text{m}$, $d_{\text{coat}} = 1{,}400\,\mu\text{m}$ and $NA = 0.5$, that is the one plotted in green,

because it allows to achieve a better power capture capability, with larger sensitivity and smaller dead end zone. For this reason, during the practical implementation of the arrangement, a fiber with these physical parameters will be exploited, as 4.1 confirms.

### 3.1.2 Single fiber simulation

The procedure is exactly the same as for facing fibers: the only difference is that now there is not a distance between the fiber cores (clearly the center of TX and RX bundles is zero, being coincident), meaning that $d_{\min} = displ_1 = displ_2 = 0$. For this reason, it is already clear that with such set up there won't be any dead end zone problem, since, at ideally zero distance from the target, the reflected light comes back completely inside the bundle.

Also in this case, the collected power can be calculated as the irradiance times the illuminated area, with the difference that, considering a single fiber arrangement, this is always constant and equal to the core of the fiber. The equations are not explicitly reported, because they are essentially the same as the previous case, with only the explained above arrangements to adapt them to this scenario.

For a single fiber sensing system, the collecting capability as function of the travelling distance is described by the equation given in 3.11.

$$P(z) = \frac{P_e}{\omega^2(z)} r_{co}^2 \tag{3.11}$$

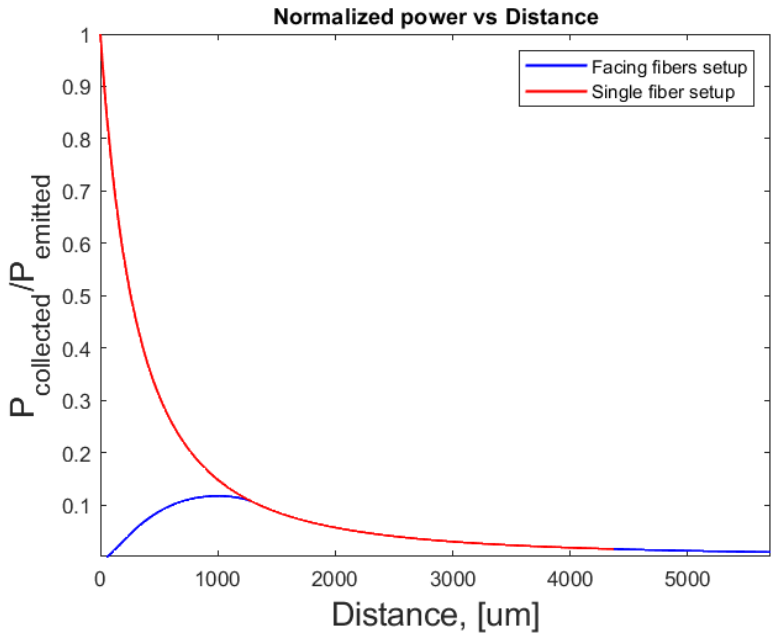


**Figure 3.6:** Single fiber vs Facing fibers power ratio

In Figure 3.6 it is possible to see how different the behavior of this kind of arrangement is with respect to the one of the facing fibers, considering fibers having $d_{\text{core}} = 1{,}000\,\mu\text{m}$, $d_{\text{clad}} = 1{,}035\,\mu\text{m}$, $d_{\text{coat}} = 1{,}400\,\mu\text{m}$ and $NA = 0.5$. As mentioned, no dead zone is present and at zero distance the power ratio is equal to one, meaning that the emitted power is entirely collected back. Another appreciable feature is that, slightly after the peak, the facing fiber setup starts behaving exactly as the single fiber exploiting the backward propagating wave. Of course this is reasonable, because, looking at the equations produced to compute the power, in the third sector (third line of the the system in 3.10) the relationship with the propagation coordinate is the same. Also conceptually, this result has a point: at that displacement, the two arrangements' cross sections in charge to collect light are fully illuminated by the beam, so there are no reasons for them to behave in different ways.

## 3.2 Matched gratings simulation

In order to understand which is the theoretical behaviour of the matched gratings, the next is to analyze and simulate which is the shift of the spectrum, (called from now on Bragg wavelength, BW) in comparison with the strain applied.

Another fundamental aspect of the simulation is to be able to analyze and choose the spectrum of the best grating. This is because, having the possibility to be able to write the matched gratings, thanks to a fs laser supplied by the Lynks laboratory, the choice of a FBG is fundamental for the research goal.

Many techniques have been tried, for example, a line by line, or a point to point engraving, with different lengths to change the reflectivity.

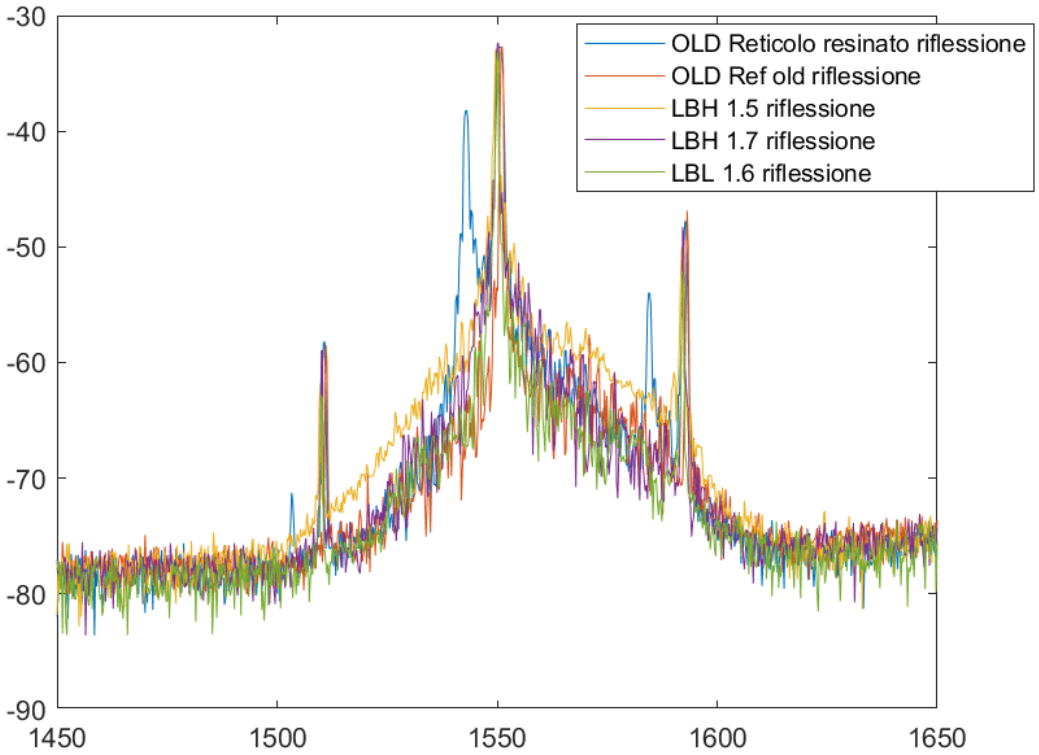


**Figure 3.7:** FBG Spectra

Figure 3.7, shows spectrum of different FBGs. These spectrum were acquired with the optical spectrum analyzer described in the chapter 2, using the GPIB driver provided by Texas Instrument. In order to acquire the data of the spectrum, a program in Python to save everything in a .txt file has been developed. To choose the reference FBG, the one with less reflectivity, but larger spectrum has been selected, and for the sensor, the one with the narrowest peak, this is because, by simulating the entire optical circuit, assuming a strain from 100 µϵ to 700 µϵ (these values are used as this is the order of magnitude of the type of vibration the system has to analyze, approximately), it gives the best results, talking about sensitivity.

Chosen the two appropriate FBG, it must be proceeded to simulate the system, considering the ideality of the optical transmission. A strain in a range suitable for the vibration measurements that the system must be able to manage was applied. The simulation was carried out by developing two MATLAB scripts, the first simulating a temperature variation, and the second is a measurement of a strain applied to the lattice.

As for the strained fiber, the considered sensitivity is, as known from literature, of 1.3 µm/µϵ, obtaining the simulation shown in the figure 3.8.

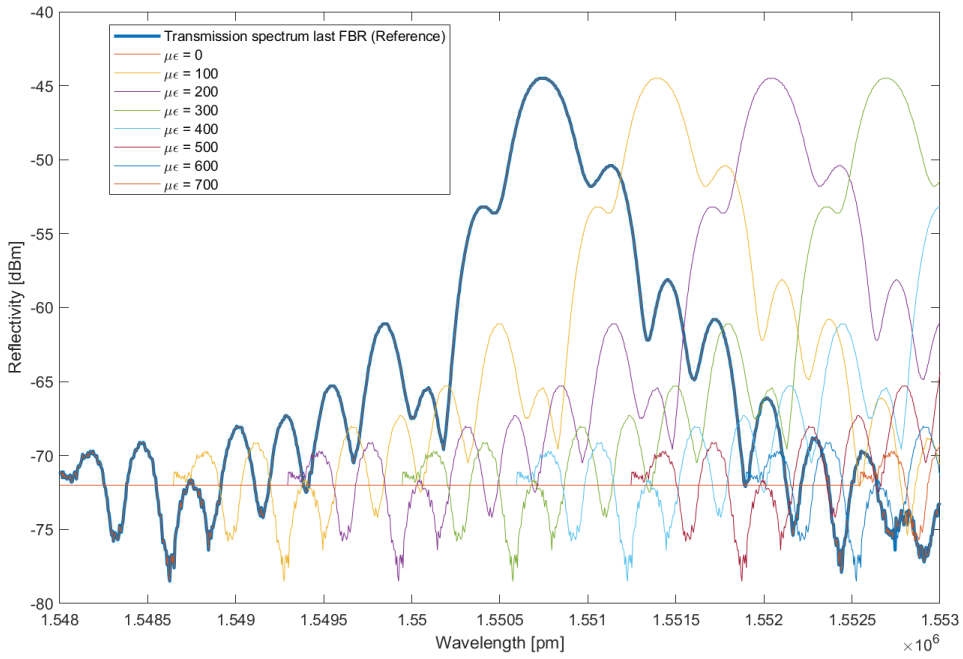


**Figure 3.8:** Strain simulation

The power received by the photodiode, can be computed as the difference between the transmitted power from the sensing grating, with respect to the reflected power of the reference matched grating. A simulation of this last computation is shown in the Figure 3.9.

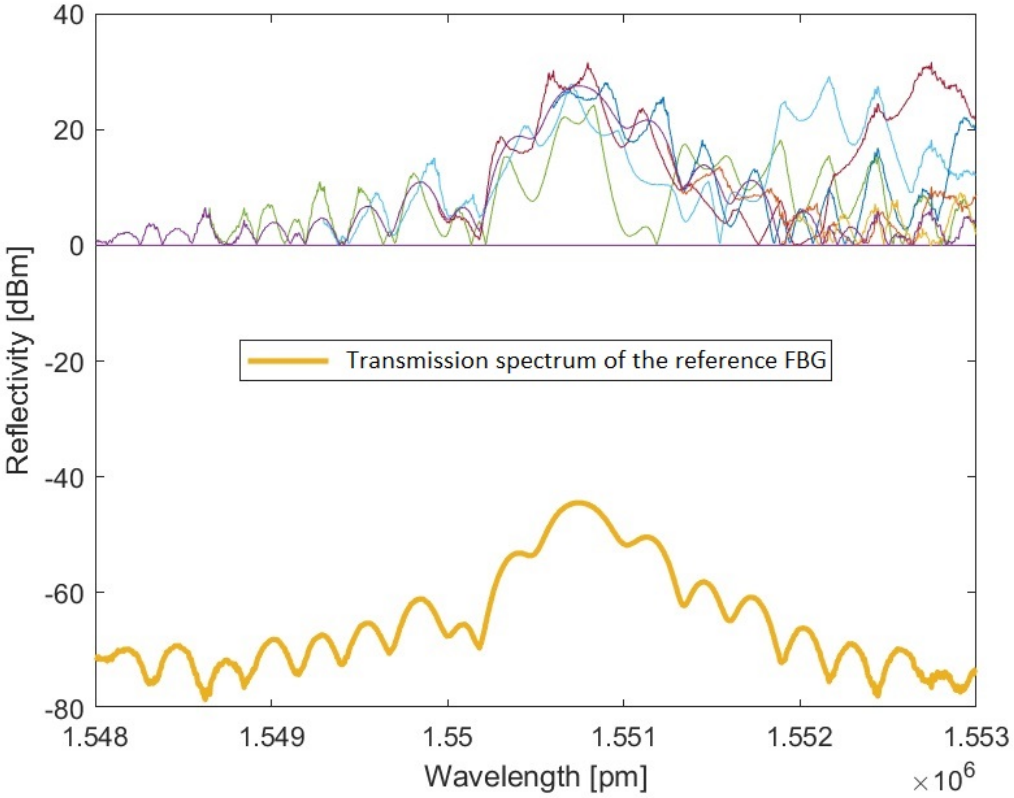


**Figure 3.9:** Power Transmitted to the PD

Then in order to have an idea of the power (actually the shape of the power), depending on the strain, the integral of the power region given by the shifted wavelength with respect to the reference one has been computed, using the "trapz" function of matlab, obtaining the normalized output power shown in Figure 3.10.

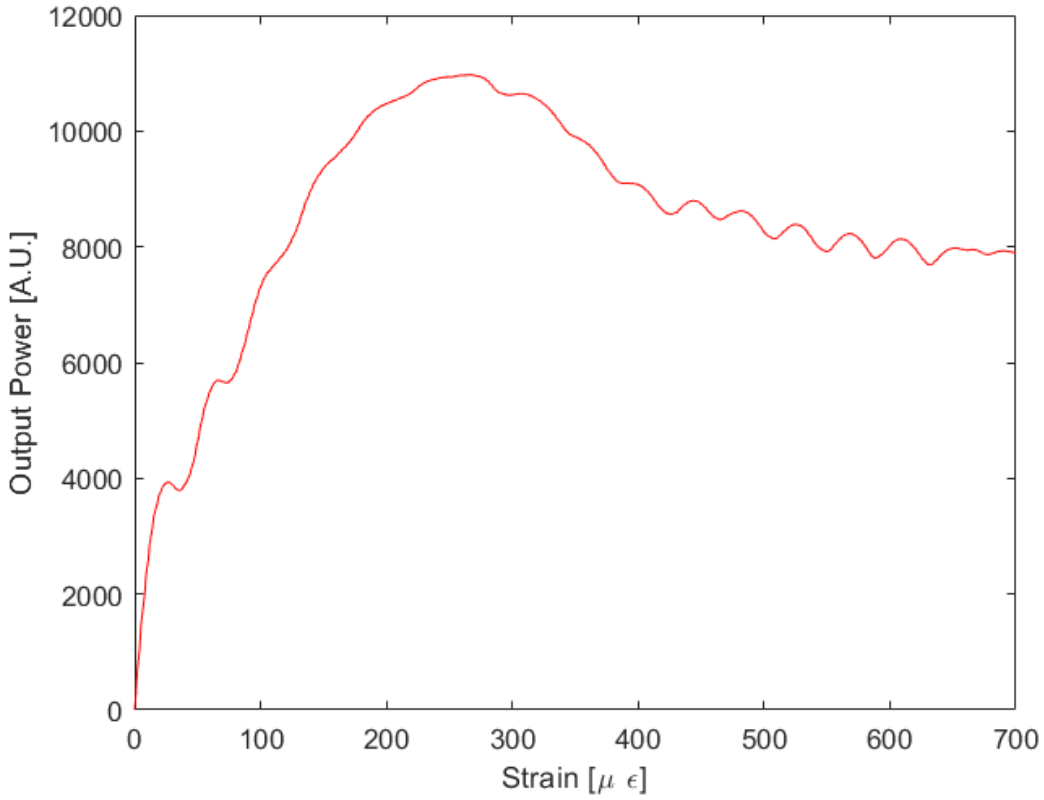


**Figure 3.10:** Output Power in arbitrary unities for the strain simulation

For what concern the temperature simulation, the idea is the same but in this case, the sensibility to consider is the one of the FBG with respect to a variation of the temperature, in the simulation case we have considered a temperature shift sensibility of 10 pm/°C, as widely known from the literature. Since the two FBG are supposed to be in the same place, the common mode of the temperature variation is simplified by itself.

From the figure 3.11, it is appreciable in the lower side of the plot, the BW shift, while in the upper side, it is computed the "useful" region for the photodiode, as in the previous simulation.

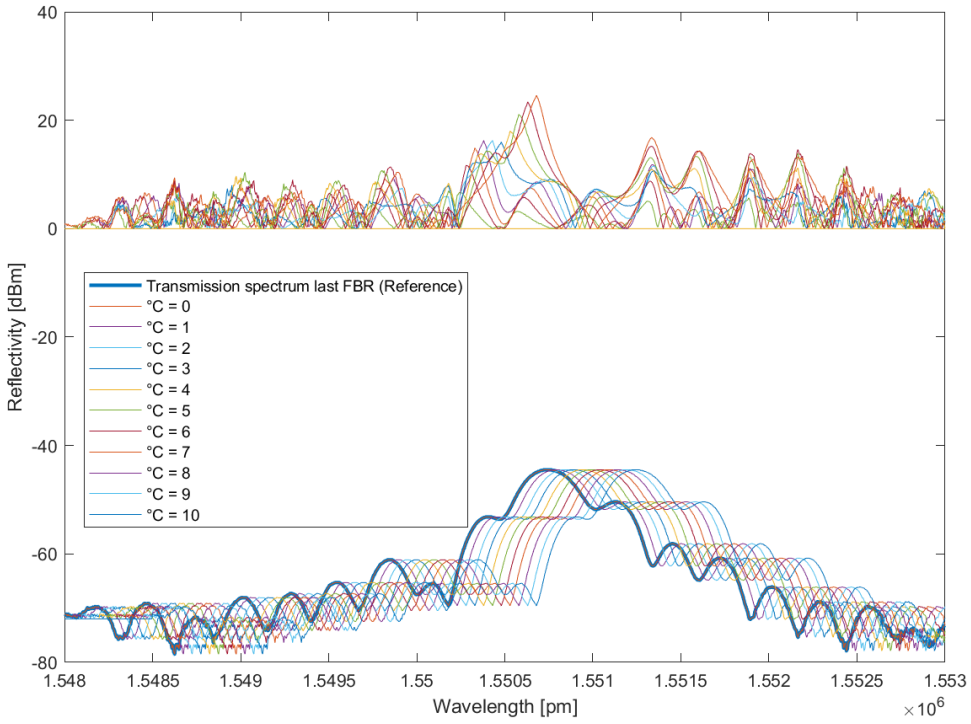


**Figure 3.11:** Temperature Shift Simulation

Then, as done before for the strain simulation, the normalized output power seen by the photodiode is computed(Figure 3.12).

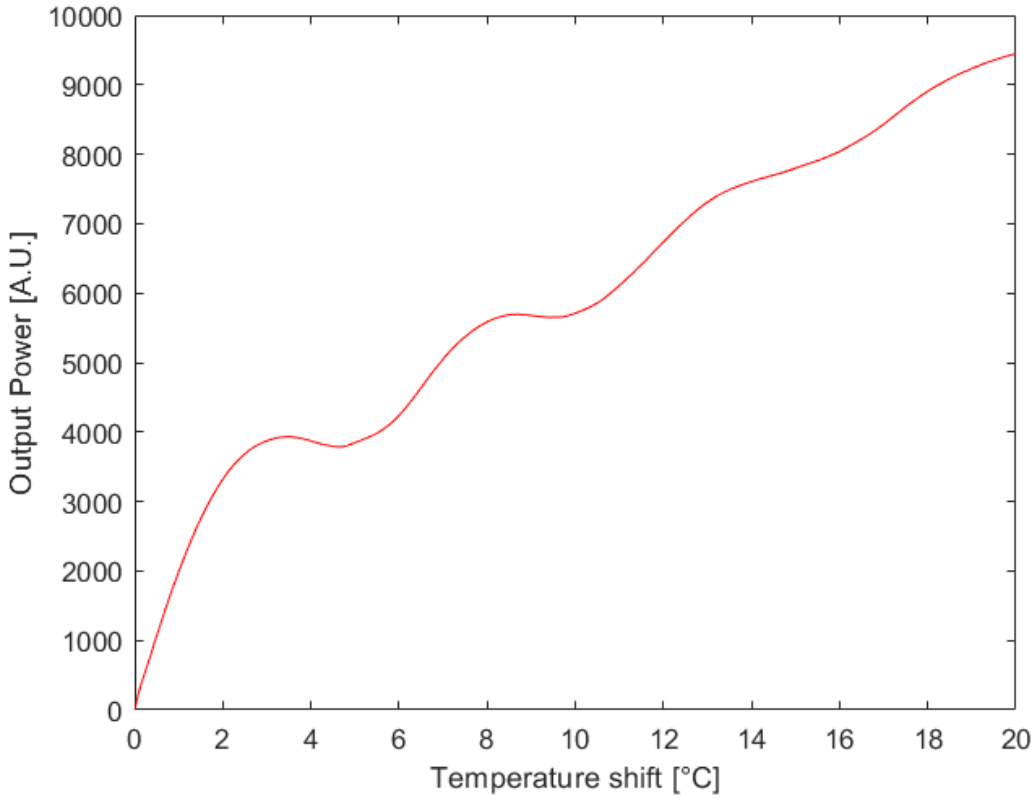


**Figure 3.12:** Output Power in arbtrary unities for temperature simulation

# Chapter 4

# Optical circuit

## 4.1 Facing fibers optical circuit

The realization of the real circuit to test the true behavior of a POF arrangement has been carried out in the most straightforward way possible: two facing fibers are placed in front of a metallic surface behaving as a mirror. This kind of setup has been chosen for simplicity, because the aim of this work is to demonstrate that facing fibers sensors can be suitable to measure dynamic displacements, so if the basic arrangement works, also more advanced ones, described in 2.1, will. In particular, the bundle is glued in a hole on a specific resonator designed by the professor Alberto Vallan and produced outside of Politecnico (Figure 4.1).

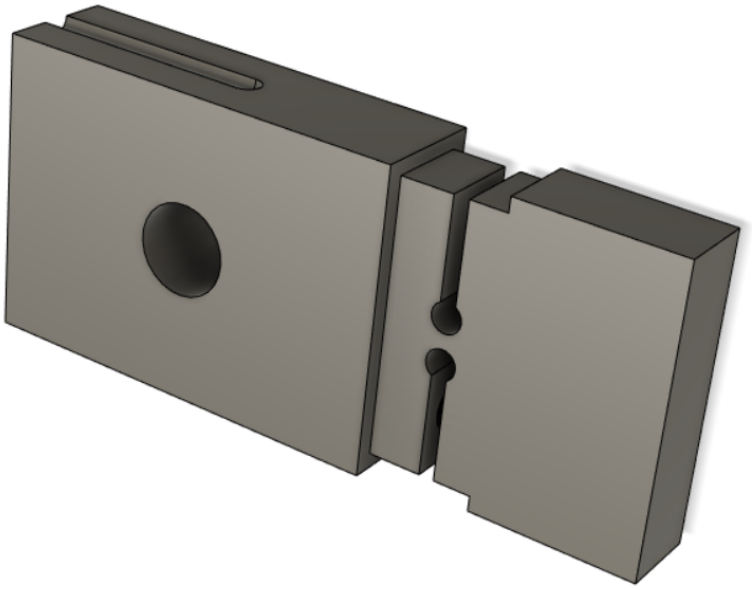

**Figure 4.1:** Resonating sensor

The fiber used is produced by Luceat SPA and has a 1,000 µm core diameter, a 1,035 µm cladding diameter and a coating diameter of 1,400 µm, along with a 0.5 numerical aperture. Such fiber dimensions are almost the largest commercially available and characterized on MatLAB (in Figure 3.1), this size has been chosen because it emphasizes the benefits of a plastic optic fiber: having great cross section and numerical aperture allow the fiber to guide many millions of modes, so it can collect the most of the incoming light. Off-the-shelf, also fibers with core diameter of 1.5 mm are available, but the connectorized LED and photodiode exploited are suitable up to 1 mm diameter.

Two different fibers are required (one to transmit and one to receive), so a total of four extremities have been lapped thanks to the polish equipment provided. This box is composed by a POF cleaver to already cut the fiber in a plane way and by several abrasive plastic sheets of different grains to polish the surface with increasing roughness, making it uniform and smooth. After having performed this procedure on all the 4 leads, the result is that the fibers perform a less lossy behavior, acting more like the ideal case of an, in principle, neat cross section, without impurities or grains that may reflect back a portion of the incident light.

The two fibers are stuck together at the sensing lead and split in the second end, where there are the LED and the photo-diode integrated into a fiber connector. These components are manufactured by Ratioplast and are called $T05EM850SM119$.

The LED is powered by the battery pack supplying also the printed circuit board, while the photo-diode is connected to the electronic part of the device, since the

sensed signal brings information in the current exiting from it. To better describe this set up, a schematic of what explained above is attached in Figure 4.2.

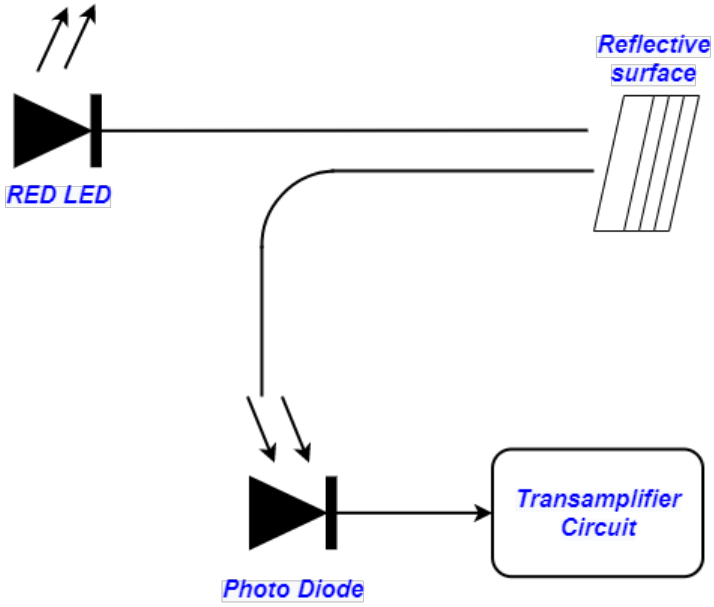


**Figure 4.2:** POF based sensor sketch

The distance between the two POF and the resonator is set to 1.7 mm. According to the simulations previously exposed, the power and sensitivity to distance ratios for the fiber exploited are the ones in Figure 4.3 and Figure 4.4. As the marker on the pictures shows, the chosen distance is well suited in the center of the most linear region in the power curve, which also corresponds to a decent sensitivity value on the second graph. To design a sensor that is capable to measure both strain and compression, it is required to place the rest position at a distance that is in the middle of the falling area. This choice leads to the fact that a reduction of the distance produces larger collected power, while an increase gives a smaller conveyed light, because the sensor is operating in the negative sensitivity region.

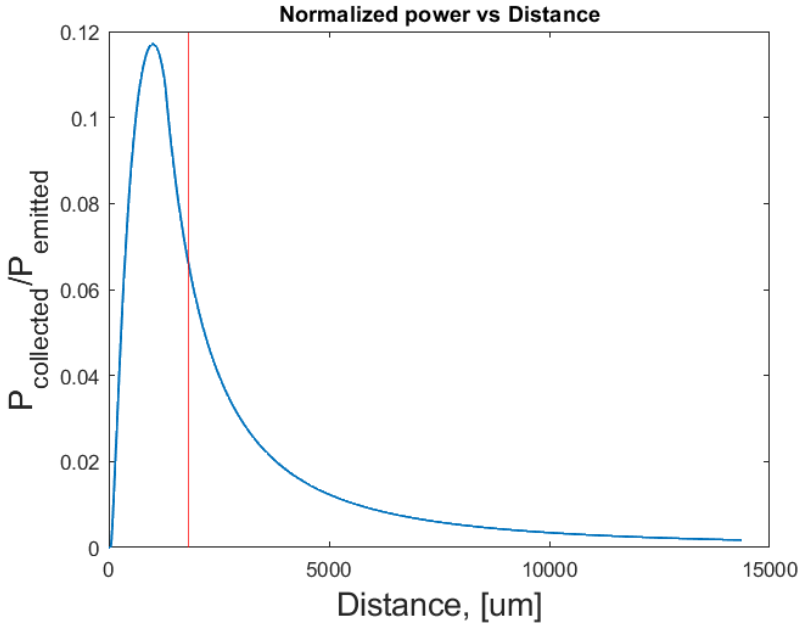


**Figure 4.3:** Normalized power versus distance for the exploited fiber

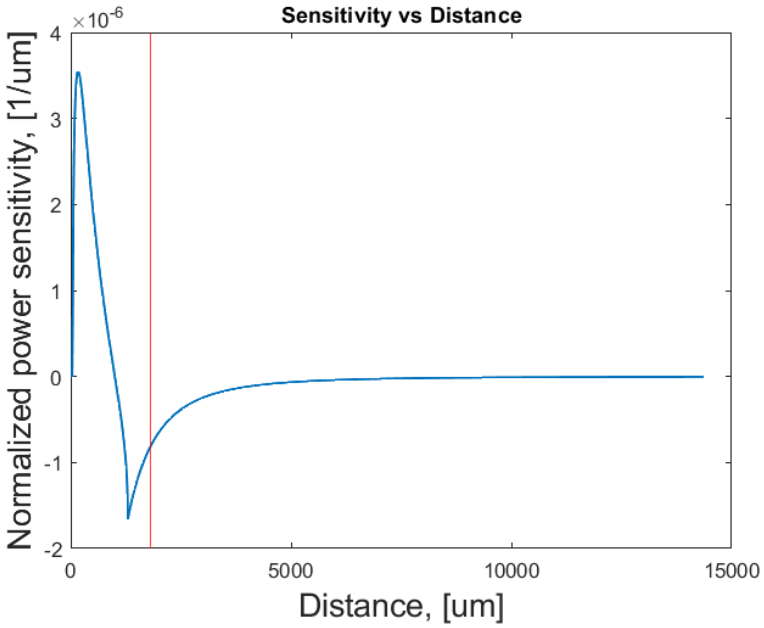


**Figure 4.4:** Sensitivity versus distance for the exploited fiber

## 4.2 Matched gratings optical circuit

The optical circuit exploited in the Bragg gratings version of the sensor is the one represented in the schematic of Figure 4.5.

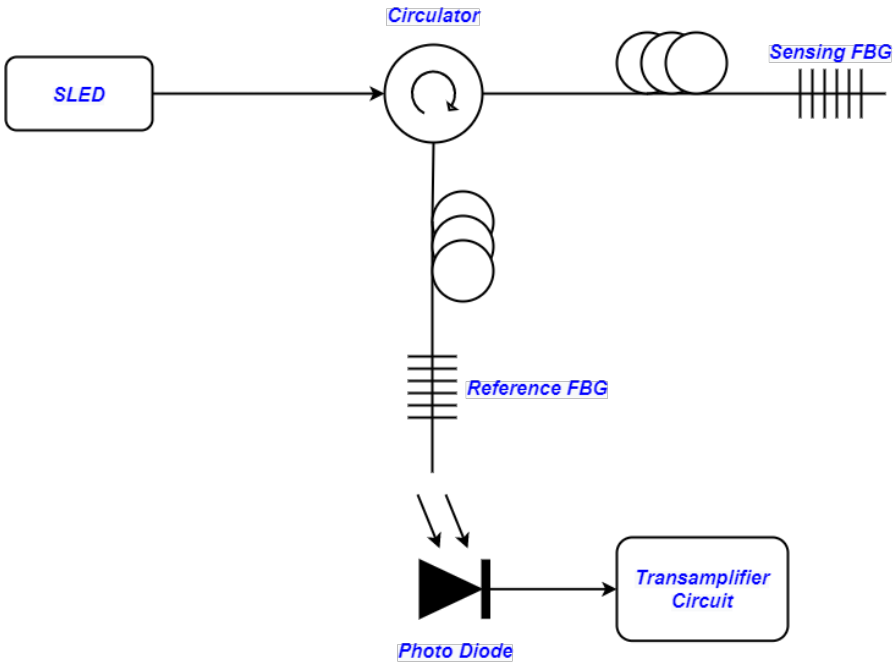


**Figure 4.5:** FBG sketch

The required components for this arrangement are: a single mode fiber coupled broadband source, a circulator, two identical FBG written on two different fibers and a fiber coupled photodiode. Furthermore some optical connectors and patch cords may be required to match the terminations in the fiber leads and to form junctions.

The optical source exploited is the Thorlabs Fiber Coupled SLD source (1550 SM), that emits a single mode on a wide frequency band centered at 1,550 nm. This device is particularly well suited, because the frequency shift caused by the Bragg Grating is orders of magnitude smaller than the band in which the light is emitted, so it covers the entire region where the wavelength swings due to external strains. Figure 4.6 shows the spectrum of the provided source. Inside this device, the light is already coupled into a fiber and it is available from the outside through a pigtail.

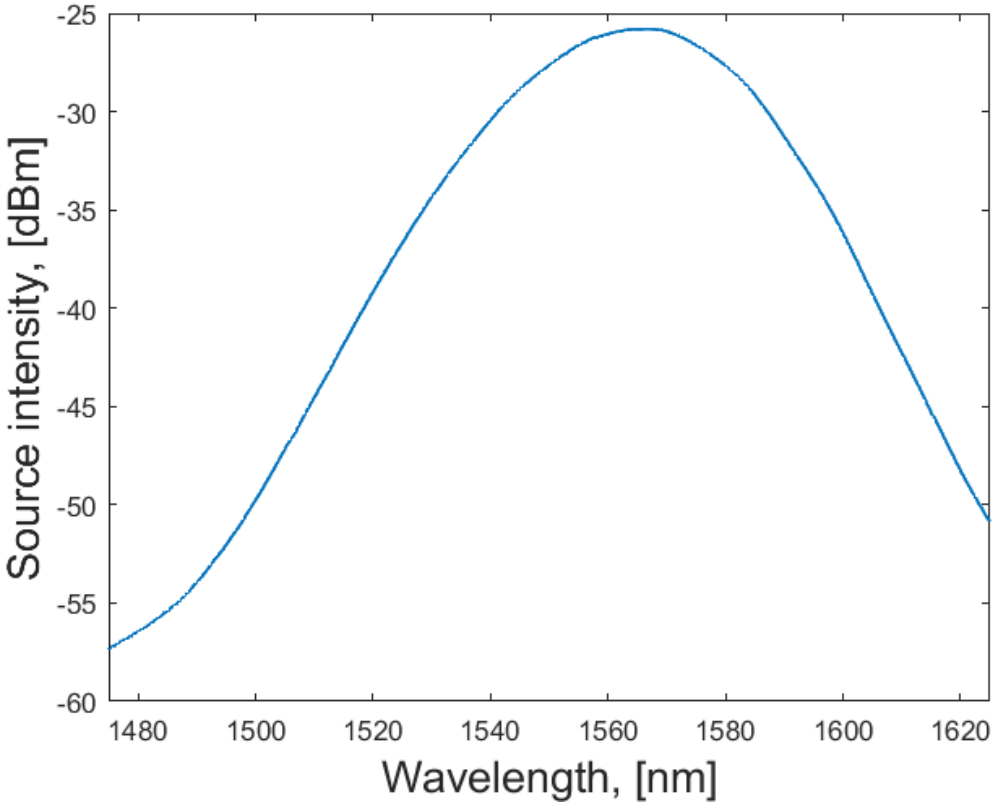


**Figure 4.6:** Source spectrum

The two identical FBG are produced in the Links laboratory at Politecnico di Torino and have nominal resting Bragg wavelength $\lambda_G = 1{,}550\,\text{nm}$. The two are only ideally twin, indeed their spectra are clearly different, but they meet the necessary condition of having the two main peaks superimposed. The frequency response of the two Bragg Gratings are reported in the figure below (Figure 4.7). In principle, the reflectivity peak can be placed at whatever wavelength, but, as a design choice, it has been placed at the center of the third telecommunication window, so, in this way, TLC component, that are more affordable, are suitable for the application.

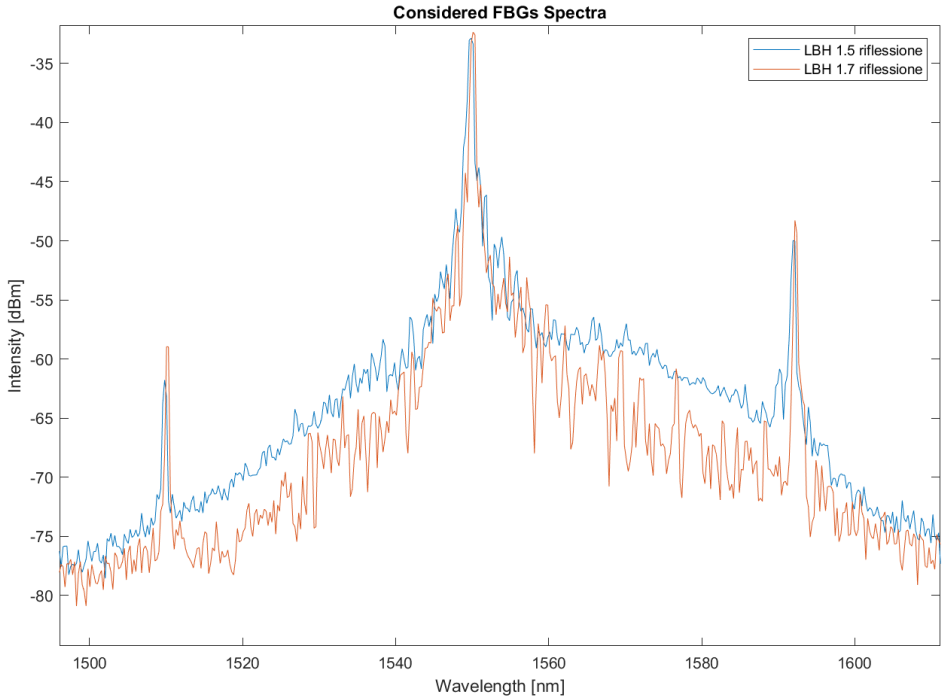


**Figure 4.7:** Gratings spectra

The operating principle is the following: the source is connected to port 1 of a circulator, letting the light flow to port 2, where the sensing FBG is connected to acknowledge external strains. In this way, the Bragg wavelength shifts according to external environment: the reflected signal is only a small portion of the one provided by the source and its frequency carries the meaningful information. The reflection returns back to the circulator entering from port 2, so it exits at port 3, where the reference FBG is kept without perturbations. If the two gratings are placed next to each other, as they are, there exists a further benefit: they always perceive the same temperature and the shift it causes is the same for both, meaning that the two peaks move together, resulting in a null effect. In this way the temperature changes are in common mode and can not affect the measurement, having canceled its sensitivity on the probing fiber.

Regarding the second FBG, the transmission through the grating is considered, indeed its output is connected to the photo-diode that converts the light flown up to there into a current. That is the last component of the optical part, since it is then soldered on the PCB of the electronic circuit, whose aim is to acquire data from the sensor.

Being the two gratings nominally equal, if no strains or contractions are applied, the signal should be almost null, since the two reflect back the same frequency, so the transmission from the reference fiber is ideally zero. If, instead, the sensing

FBG is facing a perturbation, its Bragg wavelength shifts ending up slightly miss matched with the second: a portion of the reflected light is capable to pass through the reference, leading to an increase of optic power able to reach the photo-diode. By increasing the strain or contraction magnitude, the two Bragg wavelength are even more separated, letting more light flow to the electronic circuit.

The only issue arisen is that both a positive and negative strain causes the same behavior in terms of output power, therefore a constant prestrain has been applied to the sensing fiber. This small known displacement allows to achieve a steady non zero output current in rest conditions, while strains and contractions are sensed as, respectively, an increase or a decrease from that level.

In order to have an easy comparison between the two sensor arrangements (FBG and POF based), the sensing fiber is glued on the same resonator (Figure 4.1) hosting the POF version, but placed in a different manner: the grating is placed as a bridge between the fixed part and the moving one (working as the mass of the mass-spring-damper system). Being fixed in that position, the sensor is capable to monitor the resonator vibrations and convert them into a variation of the reflected wavelength.

A picture of the set up described above is given in Figure 4.8.

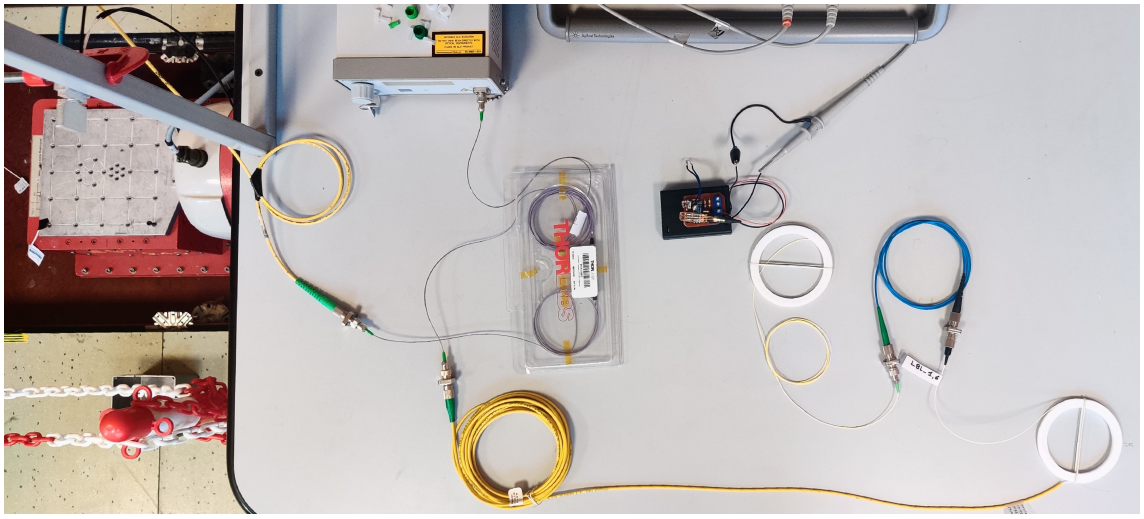

**Figure 4.8:** FBG setup image

In Figure 4.9, it is appreciable the arrangement of both the POF and FBG version of the optic circuit, since as already pointed out, the resonating tool is the same for both applications.

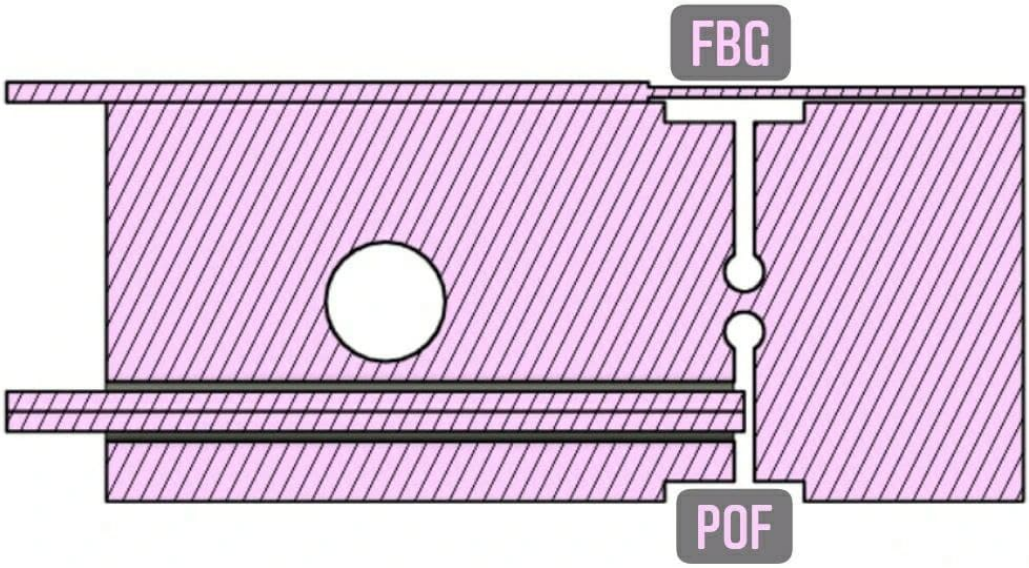


**Figure 4.9:** Resonating sensor lateral cross section

# Chapter 5

# Analog electronics

## 5.1 Facing fibers analog circuit

The electronic circuit has been designed on a PCB: the layout has been created with a software called EasyEDA, then it was passed to a CNC milling machine that has produced the board shown in Figure 5.1.

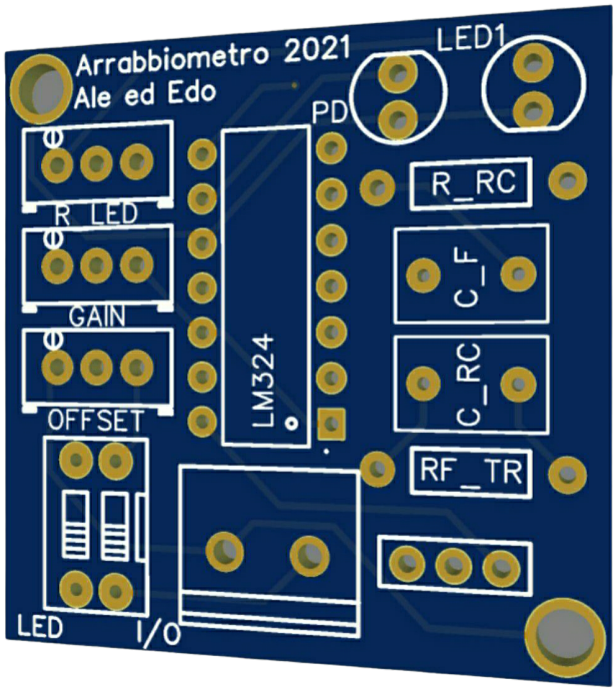


**Figure 5.1:** Facing fibers PCB image

Since the power supply available in the LEDs laboratories is responsible of a significant amount of noise coming from the main power, the entire electronic circuit (both the analog and the digital parts) is powered on by a 4.5 V battery pack. This trick reduces substantially the noise seen on the oscilloscope that is affecting the measurements, because the new power source is capable to supply a steady and stable voltage. The only drawback is that the battery cells run out of charge and should be replaced periodically. In order to attenuate the discomfort coming from this design choice, two switches have been used to turn off the entire system or just the LED, that is the most energy demanding component. The battery pack exploited is provided of only two wires, the ground and the positive supply voltage, meaning that the amplification circuit has to be unipolar, indeed some offset are required, as widely explained later on.

Being the output power level coming from the optical part very low, it is required to amplify the signal so that it reaches a voltage level adequate to be the input of the microcontroller's ADC. For this task it is important to not reach the saturation of the OP-AMP: for this aim, the total amplification has been achieved by means of three different stages in cascade configuration. Later in his section, when the design choices are explained, it will be clear the reason why the amplifying process has been split in three different OP-AMP.

Since the input impedance of the microcontroller's analog input is not so high, a further amplifier is needed at the end of the chain as a buffer to have a very large output impedance, meaning that it will not be source of problems once the ADC starts acquiring to convert the sensor signal into digital form.

Having described the specifications required by the integrated circuit, the LM324, manufactured by Texas Instruments, has been selected for the project: it consists of four independent, high-gain, internally frequency compensated operational amplifiers designed to operate from a single power supply over a wide range of voltages. The datasheet is reported in [8].

The current exiting from the photodiode carries the information about the sensed displacement inside its intensity and, since voltages are easier to manage, it has to be converted through a transamplifier. At steady state, the measured current is $I_{\text{BIAS}} = 595\,\text{nA}$, then, applying on the sensor head a strong vibration intensity in order to know the largest possible incoming magnitude, the small signal current generated by the photodiode is roughly of 0.5 nA. Then, knowing the input level, a LT Spice simulation has been carried out to design the first stage: it relies on one of the 4 available amplifier and it is just a resistor of 4.7 MΩ resistor placed in the feedback with a capacitor of 2.2 nF in parallel used to remove noise and insert a pole to limit the band. The source considered is an ideal current generator producing a sinusoidal wave with DC and AC components of the values mentioned above. Figure 5.2 shows the circuit schematic and the graph of the output. In this way, the output of this stage is a voltage, so now it has to be manipulated to bring the swing to a more suitable range.

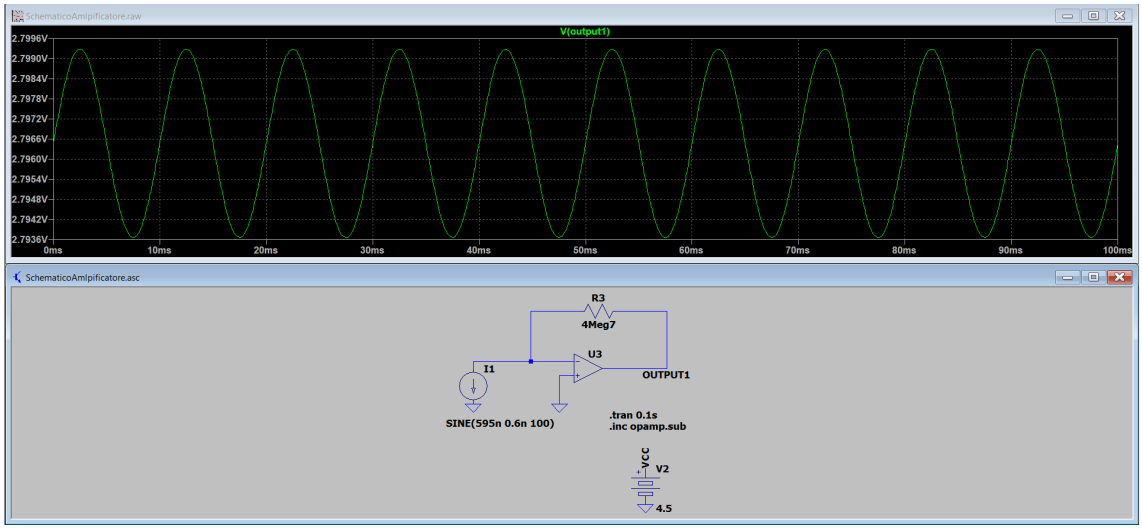


**Figure 5.2:** Spice simulation of the first stage

As appreciable, the sine-wave is now oscillating around a BIAS point of $V_{\text{BIAS}} = 2.796{,}6\,\text{V}$, with a dynamic swing of $V_{\text{PP1}} = 2.799{,}3\,\text{V} - 2.793{,}6\,\text{V} = 5.7\,\text{mV}$. Then, the signal should pass through a RC high pass filter, the resistor has a nominal value of $12\,\text{k}\Omega$ and the capacitor of $100\,\mu\text{F}$. In this way the cutoff frequency is of $0.132\,\text{Hz}$ and the DC component is removed, since for the application's purpose only the fluctuations are meaningful. The constant voltage uselessness is given by the fact that, at steady state, some light is collected by the receiving fiber, but it only brings information about the static distance from the mirror. This measure is perfectly known, being a design choice, as already discussed in the previous chapter.

Clearly, the voltage level is still not enough to achieve a decent resolution during the ADC conversion, so a further gain should be applied. Ideally, it is possible to use a single stage inverting amplifier, but in practice there are some limitation due to the elements' size this solution would lead to. Specifically, the amplification required is roughly 500 times, so, having fixed the components of the RC high-pass filter, the feedback resistor should be $R_2 = 500\,R_1$: such a large value is not recommended to be used. As an alternative, to achieve the same gain, it is possible to lower the value of $R_1$, meaning that also $R_2$ will be smaller. The drawback of this trick is that, to keep the cutoff frequency of the filter constant, now the capacitor should be larger: it already has a value of $100\,\mu\text{F}$, so this replacement is again not recommended. Hence, the solution exploiting a single stage is not the best way to manipulate the signal. As a consequence, the second stage has been split into two different inverting amplifiers on which the gain requirements are less restrictive.

After filtering, the signal goes to the second amplifying stage, but this time it is, as said, a classical inverting amplifier, that lets the voltage level reach a larger dynamics. Since the circuit is unipolar and the DC component have been removed by the filter, only the positive fluctuations could be seen, so the positive input is fed

with an offset of 2.5 V, obtained by a simple voltage partition of the supply coming from the battery pack. In this way, the bias point is placed at half the dynamics (0 V to 4.5 V), allowing to amplify both positive and negative strains with the same full scale. The LT Spice simulation is updated of the second stage as described above and gives the results shown in Figure 5.3.

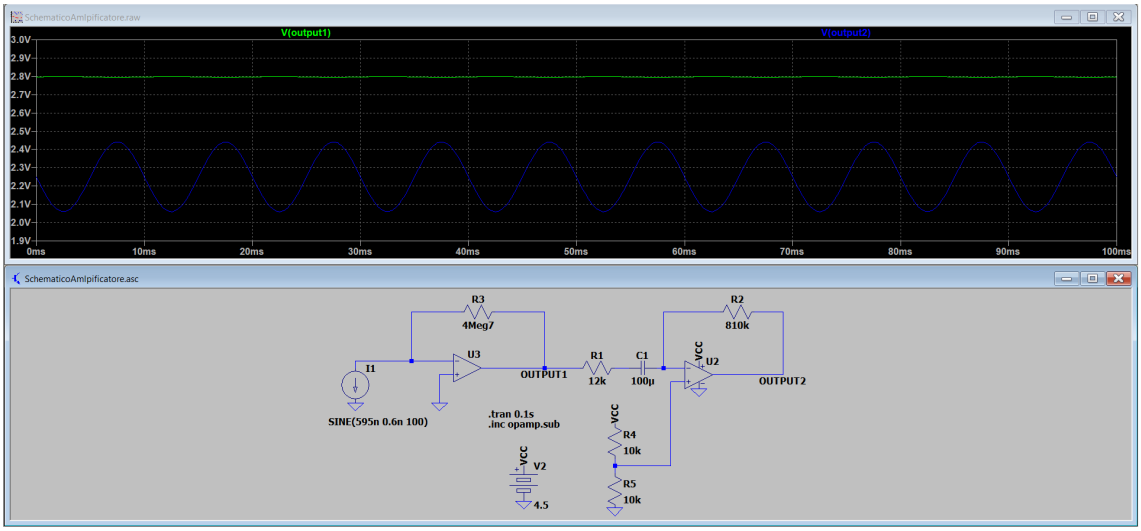


**Figure 5.3:** Spice simulation of the second stage

Designing this stage, there is already a fixed value: the resistor $R_1$ placed on the negative input is the one introduced in the high-pass filter RC group. In order not to saturate the amplifier, a gain of around 70 is chosen, so the feedback resistor should be $R_2 = 810\,\text{k}\Omega$. As from the figure, the DC component is where it is expected to be, so at half the supply level, while the voltage swing enlarges to $V_{\text{PP2}} = 2.45\,\text{V}$ - $2.05\,\text{V} = 400\,\text{mV}$.

Afterwards, a second RC filter - amplifier block is cascaded, the idea behind is exactly the same as for the previous one, with the only difference of the amplifier's feedback resistor that changes, because a different amplifying factor is required for that stage. Using the LM324 third OP-AMP, the gain applied to the output of the second RC cell is of roughly 8 times, by means of $R_1 = 12\,\text{k}\Omega$ and $R_2 = 100\,\text{k}\Omega$. The updated simulation result is given in 5.4.

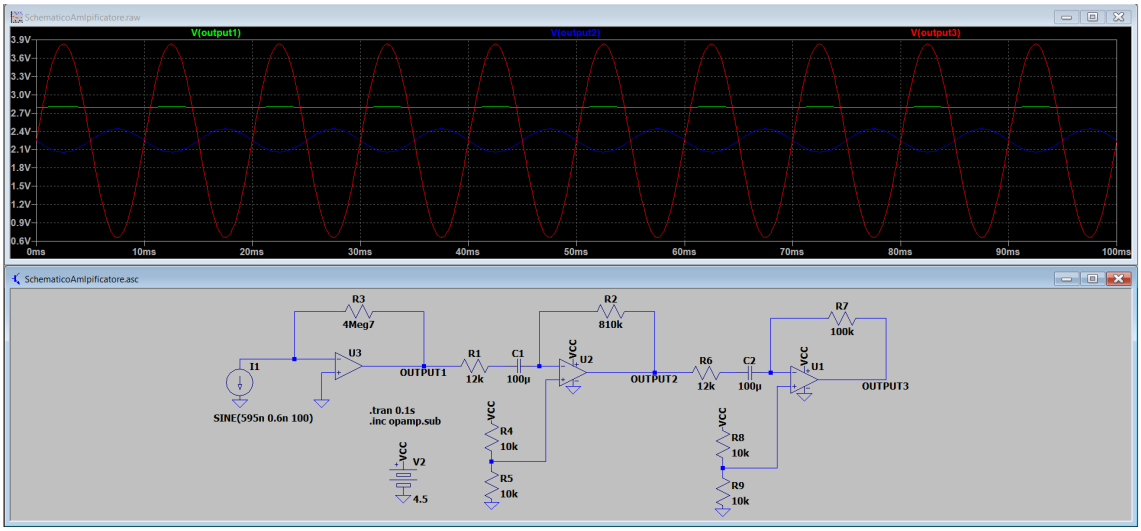


**Figure 5.4:** Spice simulation of the third stage

Now, the BIAS point is still at 2.25 V, but the small signal now has a suitable swing to be sampled by the 0 V to 4.5 V ADC input of the microcontroller, that is of $V_{\text{PP3}} = 3.85\,\text{V} - 0.65\,\text{V} = 3.2\,\text{V}$.

As previously mentioned, the last OP-AMP is then used to increase the output impedance thanks to a buffer. The entire circuit schematic is reported in Figure 5.5.

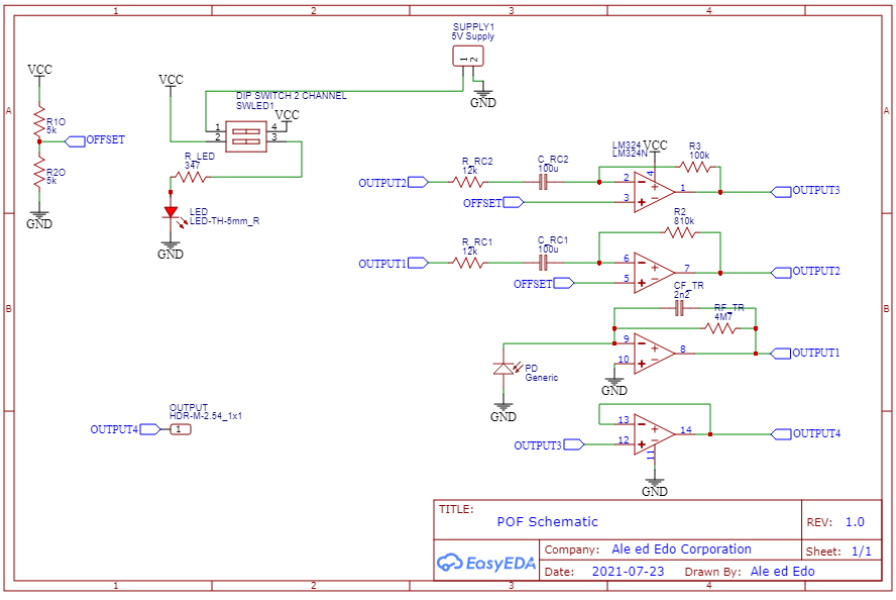


**Figure 5.5:** POF based sensor's analog circuit schematic

As a last simulation, the frequency response of the entire circuit was considered. The graph was again produced using LT Spice, setting a frequency sweep from 0.01 Hz

to 100 Hz and considering 100 points per decade. This plot has been produced in order to appreciate how the poles and zeroes inserted by the capacitors affect the bode diagram of the output with respect to the input: the two RC high pass filters, being sized with the same components, are responsible for two coincident zeros which determine the lower limit of the pass band. Conversely, the reaction capacitor in the transimpedance amplifier produces a pole, on which the upper limit of the -3 dB band depends. The pole and zero are computed with the equation 5.1.

$$f_{\mathrm{p/z}} = \frac{1}{2\pi RC} \tag{5.1}$$

The pole is placed @15.4 Hz, while, as already pointed out, the double zero is placed @0.132 Hz. Regarding the upper cutoff frequency of the band, the intrinsic low pass filter behavior of the OP-AMP has been neglected, since the pole it introduces is at a way higher frequency with respect to the one given by the circuit.

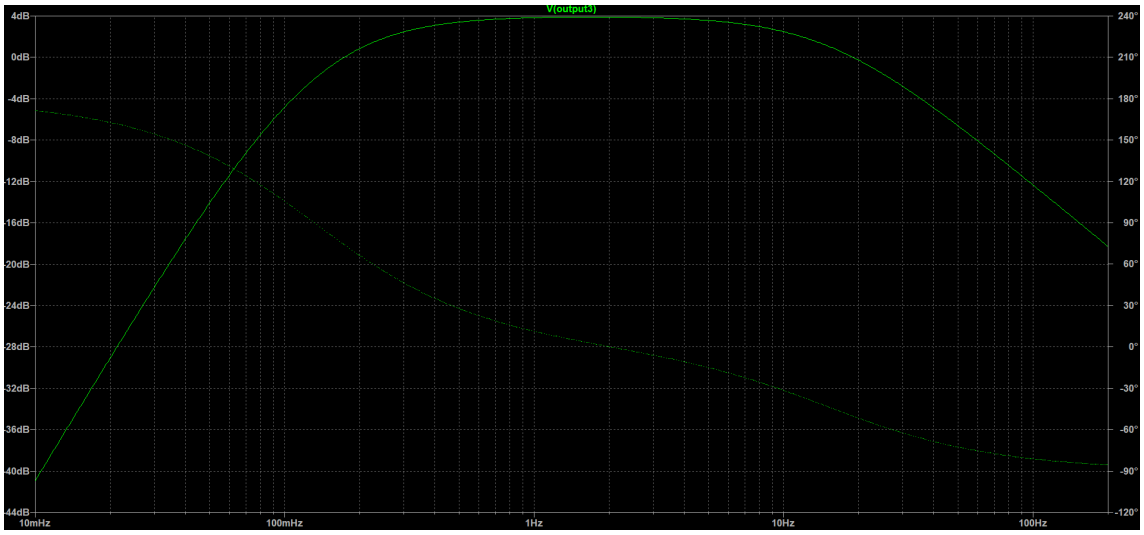


**Figure 5.6:** Circuit frequency response

By simulating the frequency response of the circuit, the graph shown in the figure is obtained, it conforms to what is expected: the module (continuous line) shows a band-pass behavior, with a rise of 40 dB/dec and a descent to -20dB/dec. This result is reasonable, as there is a double zero and a single pole in the circuit.

The circuit produced as a first prototype, just to check that everything works fine as it was designed is shown in Figure 5.7. The components used are the old through hole, since it is only an intermediate step toward the final result, so the size of the board is not a pressing requirement.

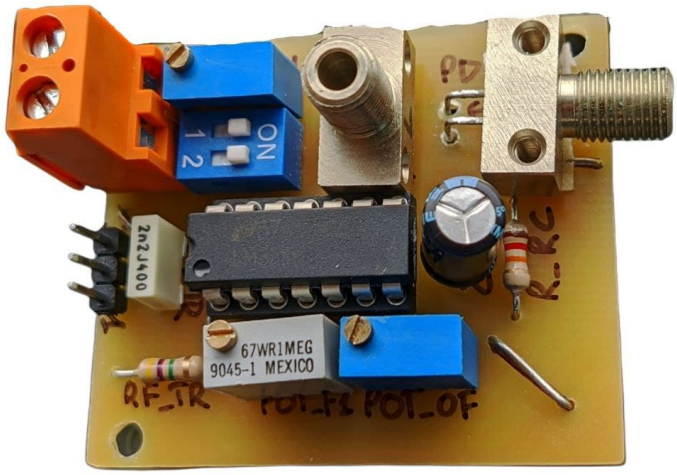


**Figure 5.7:** Circuit prototype picture

After having verified the correct functioning of the prototype PCB, to reduce the spatial occupation of the analog circuit, the layout has been designed to host resistors and capacitors in SMD technology. This trick allows to reduce the dimensions by at least a half with respect to the prototype ones. Resistors and capacitors SMD series used is the 0805. As appreciable from Figure 5.8, there are some exceptions in the sensor final realization: the 100 µF capacitance of the RC high pass filters exceeds the values available in SMD technology in the laboratory, so an electrolitic capacitor has been exploited.

Furthermore, being the input current in the order of nA, the gain of the first stage (transimpedence amplifier) have been chosen to be the largest possible. This can be a problem because the connection between the photodiode and the OP-AMP can act as an antenna collecting disturbances. For this reason, the electronic circuit has been closed in a Faraday's cage that screens all the electromagnetic interferences coming from the main power, as appreciable in Figure 5.8.

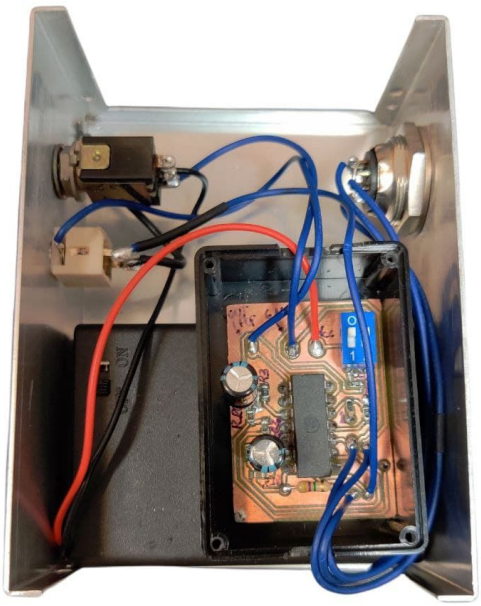

**Figure 5.8:** Image of the final PCB

## 5.2 Matched gratings analog circuit

The topic of this chapter, clearly, does not depend on the sensor technologies: what the circuit sees is the same for both the facing fiber and the matched grating optic setup, that is a photo current. For this reason, the schematic illustrated above is suitable also for what concerns the amplification of a signal coming from an optic sensor exploiting an FBG based sensor head. Having different input current values with respect to the other application, it is required to change the gains of the three amplifying stages, in order to reach a proper range of voltage, that can be kept inside the 0 V to 4.5 V microcontroller input dynamics. To do this, it has been required to modify the components used, but the PCB design layout is still the same for both the prototype and the final circuit.

Here below are reported the only features that have been changed:

- First stage (transimpedance) gain: from 4.7 MΩ to 51.6 MΩ (composed by 6 8.2 MΩ resistors in series);

- RC low pass filter components to obtain the same pole as the one of the previous section ($\cong$ 10.5 ms);
- First RC high pass filter time constant: from 1.2 s to 10 s;
- Second stage gain: from 67.5 times to 4.5 times;
- Second RC high pass filter time constant: from 1.2 s to 0.22 s;
- Third stage gain: from 8.3 times to 45.5 times;

The resulting schematic, for what concerns the changes listed above, is presented in Figure 5.9.

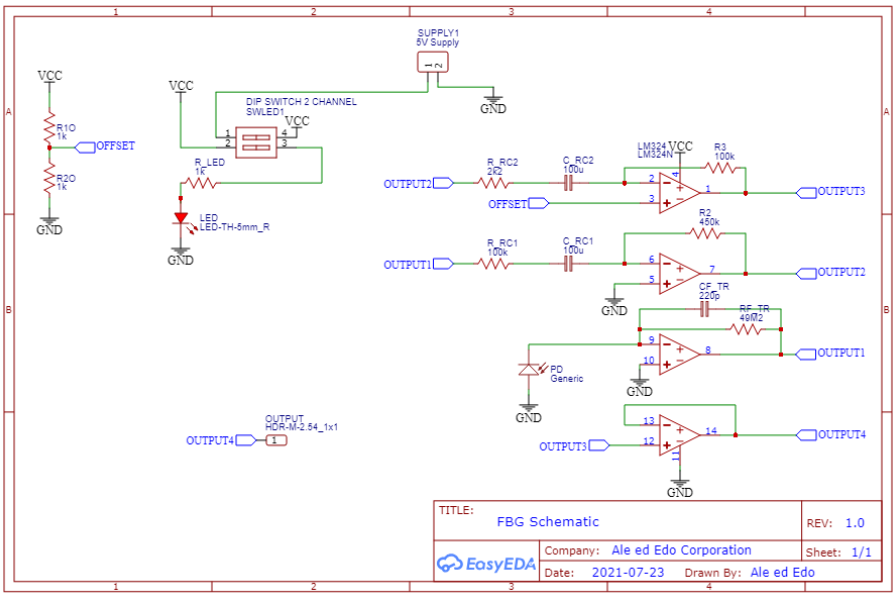


**Figure 5.9:** FBG based sensor's analog circuit schematic

# Chapter 6

# Digital electronics and microcontroller

The next step to design is the digital electronics circuit that allows to acquire the signal exiting from the amplifiers and to transform it in a digital sequence that can be understood by the PC, by which we would like to show data coming from the optic sensors. Again, this section is no more dependent on the sensor technology used, but it has to be universal, so that both the facing fibers or matched gratings based sensors can be connected to the same interrogator and the user can work regardless on which one of the two. In order to acquire the signal coming from the transamplifing circuit, it has been used a micro-controller based on the Atmega328p Chip, in particular, the Arduino Nano board, later on the choice will be motivated.

## 6.1 Micro-controller

The Atmega328p has a built-in multichannel, 10-bit analog to digital converter. This means that it will map input voltages between 0 and the operating voltage (4.5 V from the battery pack) into integer values between 0 and 1023, so it yields a resolution between readings of roughly 4.5 mV per unit.

Considering to achieve high sampling speed, it has been necessary to work at the register level, in order to configure the timer and the ADC.

First of all, some considerations should be done: the analogRead() function provided by the Arduino library is not compatible with the project, because it has a lot of built-in functions (for example to control if the Analog Input is the correct one), which dramatically increase the delay between one sample and the next one. Another key aspect of the program, is to give priority to the sampling instead of any other instruction, in order not to lose any important sample: to do so, it is necessary to work with the Interrupt Service Routine (ISR). An ISR is a software routine that hardware invokes in response to an interrupt, in our case, it's called directly from

the timer of the ADC. ISR examines an interrupt and determines how to handle it, in particular, the routine is composed by only two instruction, the allocation of the analog read in a variable called adcReading and the assignment of a boolean variable, which is read by the main loop in order to understand that a new sample is ready to be analyzed.

## 6.2 ADC

Since the ADC has a 10 bit resolution, the value red is between 0 and 1023, meaning that at least a two bytes variable is required. In order to communicate with the PC,the micro-controller used, provides different functions for the serial transmission, but it will be covered in the next chapter (7).

Regarding the clock configurations, in order to sample at high frequency, but without loosing in resolution (we want to take care of at least 10 bit of resolution), we set a prescaler of 128. With these configuration, considering that our clock is at 16 MHz, the ADC conversion needs 13 clock cycles and some delay due to the communication (we'll see in details later on), leading to a sample frequency slightly larger than 7 kHz. Considering that our system is able to sense vibrations as far as roughly 200 Hz, we are completely satisfying the Nyquist theorem. The registers are configured as in the code box.

```
1  ADCSRA =  bit (ADEN);      // turn ADC on
2  ADCSRA &= ~(bit (ADPS0) | bit (ADPS1) | bit (ADPS2)); //clear
     prescaler bits
3  ADCSRA |= bit (ADPS0) | bit (ADPS1) | bit (ADPS2);// 128
4  ADMUX =  bit (REFS0) | (adcPin & 0x07);
5  TIMSK0 = 0;
```

# Chapter 7

# Communication protocols

From what concern the communication between the microcontroller (the ADC board) and the calculator, it has been decided to implement two different types of communication, serial and wireless. The first one relies on an USB wire that connects the sensor to the PC, while the second one exploits two radio modules working around 2.4 GHz.

## 7.1 Serial communication

Since for the ADC board it has been decided to use a Atmega328p microcontroller, there is a 10 bit integrated ADC capable of doing a continuous sampling with a frequency of 7.4 kHz. It has been chosen to use the Arduino Nano board, because it can work up to 16 MHz, with some tricks it should be power friendly, but above all, it has a built-in CH340 driver, with a USB Type-C socket. The CH340 is a USB bus converter chip, it can realize differential USB conversion to serial interface.

The Serial transmission is a mode of communication between digital devices in which bits are transferred along a communication channel one after the other and they arrive sequentially to the receiver in the same order in which the sender transmitted them.

Despite the greater architectural and management complexity compared to parallel transmission, the serial mode is one of the most widespread in the IT field because:

- It requires fewer wires with consequent cost reduction;
- It is more tolerant of interference and transmission errors.

As a drawback, obviously, the simpler transmission circuit has as a counterpart a greater management complexity.

The serial communication is generally sturdier than the wireless one, but it always requires to bring a USB cable to the sensor, for the majority of the cases this is not

a problem, moreover due to the fact that the cable could also bring power to the sensor itself.

In the asynchronous mode the transmitter and the receiver synchronize themselves using the data: the transmitter initially sends a starting bit, then the actual data (typically from five to eight bits, in the case 8 bits, with the least significant bit first), an optional bit of parity, and finally a stop bit which can have different typical lengths (one, one and a half or two bit times). The starting bit is of opposite polarity to the normal condition (space or 0). The stop bit is of normal polarity (mark or 1) and creates a space before the start of the next character. The standard speed for an asynchronous serial device depends on the type of data lines and is measured in bits per second (bps) or, alternatively, in symbols per second (baud).

Since the ADC samples at a frequency of 7.4 kHz, the serial communication has to transmit at a baudrate grather than 120,000 symbol/s. In order not to lose samples, we decided to set the baudrate four times higher 500,000 symbol/s.

### 7.1.1 Optimization

In order to transfer data through the serial port, there are basically two strategies, using the built-in "Serial.println()" function, which is more convenient in terms of stability and utilization, or to write directly binary data to the serial port.

The "Serial.println()" function, prints data to the serial port as human-readable ASCII text. This command can take many forms, numbers are printed using an ASCII character for each digit, in the study case, the maximum value the ADC can handle is 1023. Considering also that a "new_line" character has to be sent each sample in order to be easily understood by the Python Program in charge to plot them on screen (described in chapter 8), this leads to a huge amount of data transfer, which dramatically decreases the communication speed, making the live data-processing and plotting impossible.

Since the range of possible values sampled by the ADC is perfectly known, the serial communication can be done directly by writing binary data to the serial port. In the specific case, each sample (10 bit maximum) should be split into 2 bytes, and written directly through the serial port using the "Serial.Write()" function. In this way, for each sample coming from the micro-controller, only two bytes are required, making communication about 2.5 times faster.

Since the maximum value to send is on 10 bit, the trasmitter, but also the receiver (the Python algorithm), has to manage some computation in terms of masking and shifting (code box below), from 2 bytes in the serial buffer, to 10 bit integer.

```
1     tmp[0] = (char)adcReading;
2     tmp[1] = (char)((adcReading & 0x0300) >> 8);
3     Serial.write(tmp, 2);
```

## 7.2 Radio communication

In order to provide a more sophisticated solution, it has been implemented a wireless communication between the acquisition card (signal conditioning, dynamics adaptation, amplification, ADC) and the PC, so that the signal arriving from the fiber is analyzed. To do this two 16 MHz microcontrollers (Atmega328p) and two 2.4 GHz radio module have been exploited, specifically an NRF24L01 + module. These are radio modules with low energy consumption and really low prices. They are able to establish bidirectional communications, therefore if properly configured they could be an excellent component for a sensor network.

These modules communicate on the 2.4 GHz frequency band and with a very low energy consumption, they are able to theoretically transmit up to a hundred meters. To be managed by Arduino (ATMEGA 328p), the NRF24L01 module uses the SPI interface (Serial Peripheral Interface) The communication takes place between a master device and devices called slaves. The master (in our case the transmitter), as the name suggests, is the one who commands the communication. It manages the clock, but also it is the one which decides the right moment to open or close the communication: the wireless communication can be thought as a pipe, in which the transmitter write bytes (2 bytes for each sample, the ADC have 10 bit resolution, so we encode each sample in two bytes). The SPI communication of the module has a maximum data rate of 10 Mbps, but it is advisable to not exceed 8 Mbps.

The features of the selected radio module are presented below:

### FIFO

FIFO literally means first input first output i.e. the bit that enters first comes out first. There are 5 FIFOs of 32byte and these 5 FIFOs represent the data pipes, in addition there are 5 FIFOs for the receiver and 5 for the transmitter. In these FIFOs it is therefore possible to contain 5 packets of 32byte in reception and transmission.

### Packet form

The packet contains the information to send, but in order to work properly it needs other bytes to make a secure transmission, in particular it is made up of:

- PREAMBLE (1 byte): it is formed by the following string 10101010 and serves as packet start information and as synchronization with the receiver.
- ADDRESS (3-5 bytes): it contains the packet address and it has a minimum length of 3 bytes and a maximum of 5 bytes.
- PAYLOAD (1-32 bytes) is the actual information, the whole packet reaches the receiver but only these bytes are available outside the module.

- CRC (1-2 bytes): they are control bytes, useful as ACK, for the retransmission of the packet or as a control field for possible errors. This field may or may not be present.

The ACK is an additional packet that is transmitted from the receiver to the transmitter to inform it of the correct reception of the packet. ACK is the abbreviation for ACKNOWLEDGE.

In order to increase the communication speed, it was necessary to optimize the packet size and the communication protocol rules: the main idea is to reduce the individual size of each packet, with the aim of increase the throughput keeping the same data rate (2Mbit/s).

The payload contains the acquired sample, which is composed by 2 bytes (since the ADC has 10 bit resolution). There are two possible solutions to improve the throughput:

- to exploit all 32 bytes of the payload sending 16 samples at time
- sending one sample at time reducing the payload size to 2 bytes

To make the data management software as simple, reliable and dynamic as possible, the option number 2 is certainly the most suitable, moreover, the performances are completely comparable. Furthermore, a problem not to be underestimated is the loss of numerous samples during radio transmission, since the payload is 16 times larger, during the period in which the micro-controller is busy transmitting, the acquired samples are lost. We choose instead to send one sample at a time (and considering some precautions that we will be proposed shortly), the period in which the micro-controller is busy for transmission (about 150 us), is comparable to the sampling period of the ADC, which implies a significantly less data loss, almost absent.

```
1  radio.begin();
2  radio.setPALevel(RF24\pedPA\pedMIN);// Set PA LOW for this
   demonstration. We want the radio to be as lossy as possible for
   this example.
3  radio.setDataRate(RF24\ped2MBPS);// Raise the data rate to reduce
   transmission distance and increase lossiness
4  radio.setAutoAck(0);
5  radio.disableCRC();
6  radio.setRetries(0, 0);// Optionally, increase the delay between
   retries. Want the number of auto-retries as high as possible (15)
7  radio.openWritingPipe(pipe);
```

### 7.2.1 PCB radio fabrication

It has been designed the PCB layout for both the receiver and the transmitter, using a CAD software, specifically EasyEDA. For prototyping it has been decided to mill a

PCB using a CNC machine, because it is more robust than a circuit on a breadboard and it will avoid some disturbances and capacitance. The schematic designed with EasyEDA and the resulting board are shown in Figure 7.1 and Figure 7.2.

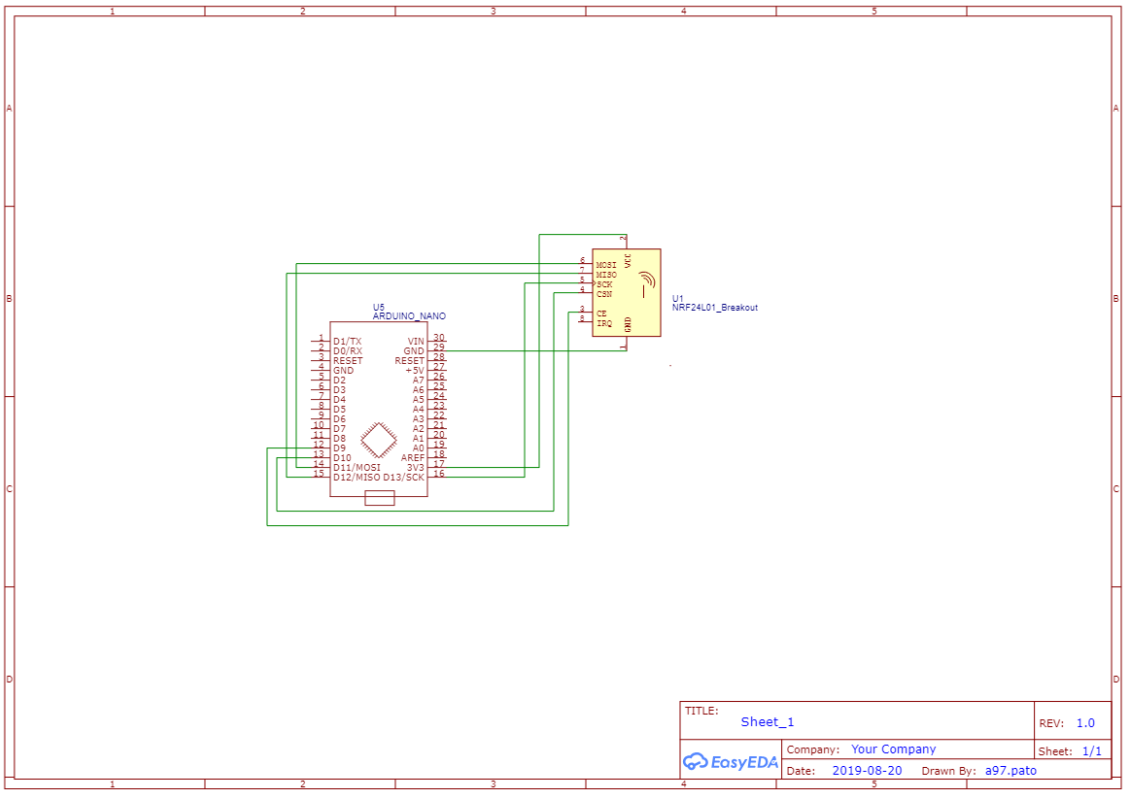


**Figure 7.1:** PCB Schematic of the Receiver

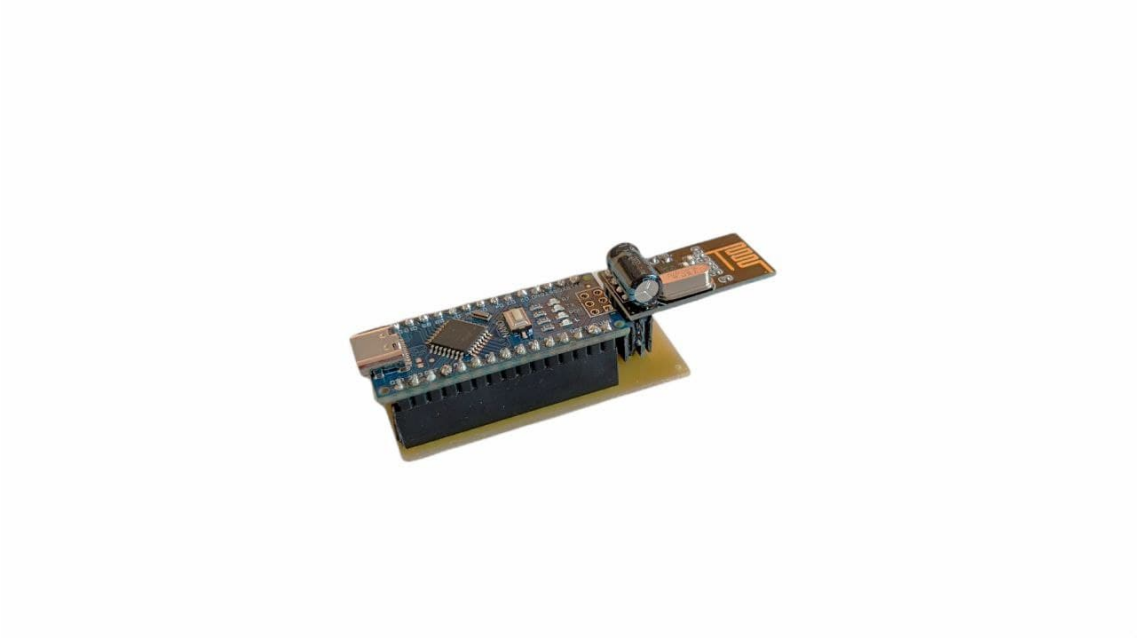

**Figure 7.2:** PCB Picture of the receiver

The transmitter PCB differ from the RX one only for a detail: it is essentially the receiver with the addition of the Microcontroller interface, that is a single connector for analog input A0. In this way it has been possible to design only a single layout and then the Arduino interface is not used at the receiving end.

For the transmitter, the use of the analog input A0 is the only connection to read the signal coming from the transamplifier circuit (signal conditioning circuit), all the others pin are exploited to manage the NRF24L01+ module.

Since the communication is done at a very high speed, and it is not very energy friendly, the NRF module needs a relevant quantity of current to communicate. If this current is not provided, the chip used by the module resets itself, causing a loss of data. In order not to loose samples and to transmit all the data to the receiver, a solution to the problem consists in soldering a 100 µF capacitor in parallel to the module power supply, as close as possible to the integrated circuit. This can help to buffer/compensate the current spikes needed by the radio module to work properly.

# Chapter 8

# Computer interface program

Once data has been collected from the microcontroller and transmitted to the PC with serial or radio communication, the next step is to develop an algorithm which can held all incoming data, manage a very basic DSP and provide to the user a real time plot.

The code is developed using Python language because it provides several useful libraries and modules to configure the serial communication and to create an efficient live plot.

The first step is to configure the baud rate, setting it equal to the one exploited by the microcontroller, and the serial port used to connect the hardware.

Since there is a huge amount of data arriving to the PC, a multi-process program is required not to create latency problems between the arriving time of the data and their live plot: this trick is very useful to avoid the bottleneck due to the serial communication. The algorithm is shown in the flow chart of Figure 8.1.

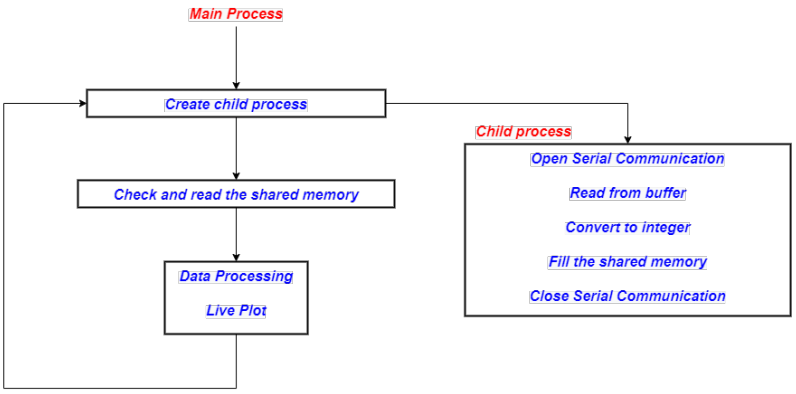


**Figure 8.1:** Algorithm flow chart

The program is developed to work simultaneously with the two processes in order to achieve the best performances. The main one (the father process) has the aim of

manage the child one and the data it provides. Moreover, its main goal is to refresh continuously a graphical user window where the live plot is shown. Once the child job is created, it has to open the serial communication with the microcontroller, read data coming from it, convert them (each sample arrive in two consecutive bytes that have to be transformed in a integer), check for errors and, if present, recover them. Once the 'data_packet' array is full (in the study case, 500 elements), the data have to be copied to the shared memory working as a queue, called 'q'.

Meanwhile, the main process has to check whether the shared memory is filled and, if so, it has to catch and plot them. In this way, samples are plotted 500 at time and in the next refresh they are all substituted by the new ones.

The multiprocessing solution has been used because a single process program is not capable of acquiring and plotting at the same time, so, while it is refreshing the user interface window, it would not be able to collect data incoming. Thanks to this trick it is possible to not loose any of the data transmitted by the microcontroller.

Furthermore, an improvement has been done to make the live plot window work as an oscilloscope in normal mode: a threshold is defined and, when a data exceeds it, it is considered as the leftmost element of the window plot (i.e. it is the first of the 500 shown simultaneously in the user interface). By properly choosing the threshold just above the noise floor, this feature will not trigger without external perturbations, so the program works in its most basic way. On the contrary, if a vibration is detected, the program will show it and hold it on screen for a time pre selected by the user.

# Chapter 9

# Measurements

After having designed entirely the two systems, they have been widely tested to verify their correct functioning and to correct the imperfections in the several parameters (as, for example, amplifiers gain, correct distance from the reflecting surface for the facing fibers or the required pre-strain for the matched gratings setup).

Firstly, the Python software and the communication types have been checked. The test has been done by applying an external vibration on the sensor head and on the live plot it was appreciable how the software is capable to follow the resonance of the mass-spring-damper system.

Once it has been confirmed that the system's digital section is working as expected, the focus switched to the entire previous part, comprehensive of the sensing optical head and the analog conditioning circuits. For this aim, the signal generated by external perturbations have been acquired with a digital oscilloscope, so that its full scale ranges provide on screen how large the amplitude is and how fast in time the signals are. This is due to the fact that the python software is capable to only plot a qualitative shape of the perturbations, while, in a more detailed analysis, it is also required a quantitative evaluation of the vibration measured. In the oscilloscope screenshots presented below, it is also shown how all its parameters are configured, so it is possible to compare the magnitude of the several tests performed to the system.

## 9.1 Single system features

This section presents some types of measurement examples that the system can handle. During these tests, only one of the two sensing devices have been exploited, but of course both of them are capable to acquire such signals. This is just to avoid messy images, with 2 signals and different scales to just see a replica of the signal. The comparisons between the two arrangements are widely discussed later in this chapter.

The first sample under test is a vibration monitoring system for an air compressor on which the sensing element has been fixed on the chassis to keep them jointly

liable.

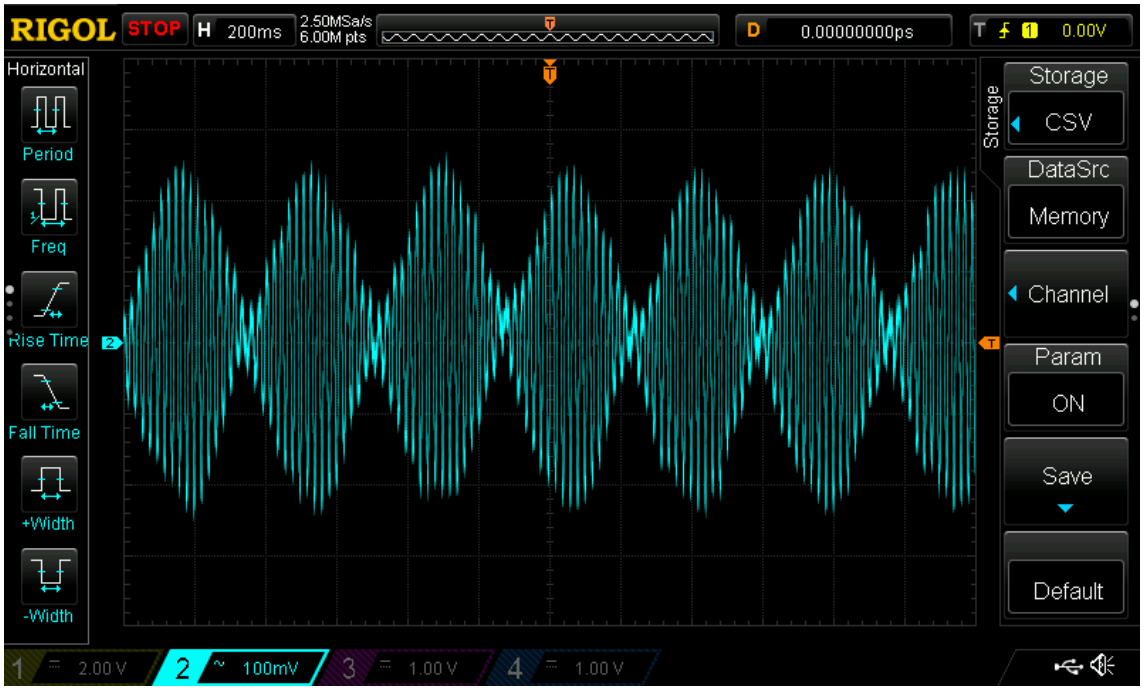


**Figure 9.1:** Air compressor vibration in time domain

As appreciable from Figure 9.1, the system is capable to measure both fast and slow variations: indeed, the acquisition shows an amplitude modulated signal. Once it was sampled, data have been processed to obtain the FFT, in order to analyze spectral components of the considered vibration. The spectrum is shown in Figure 9.2.

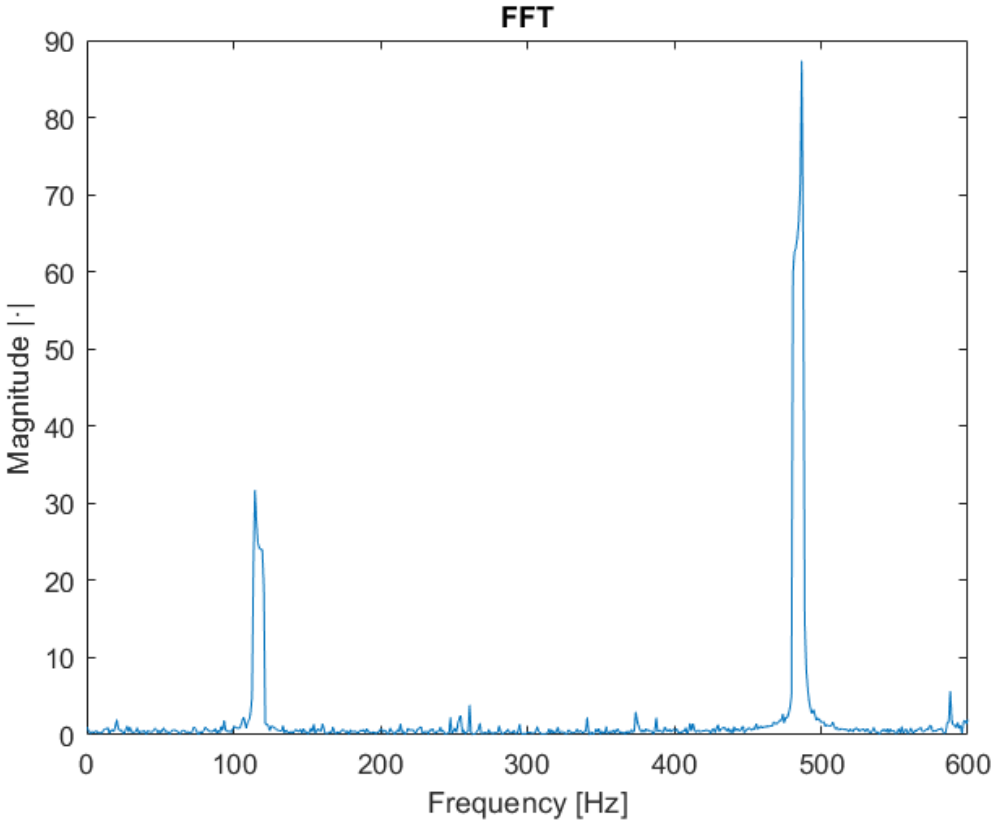


**Figure 9.2:** Air compressor vibration in frequency domain

As the figure shows, there are two main spectral components, as expected from the time domain behavior: the first one is around 115 Hz, while the second is roughly at 535 Hz.

This kind of measurement has been presented because it shows in a clear way how the system is capable to appreciate both fast and slow frequency components, and also it confirms its capability in terms of bandwidth.

Another type of purpose the system can perform, is the capability to analyze the resonant frequency of a particular device under test. In the study case, the object is the resonating sensor described before, which acts as a mass-spring-damper system.

As appreciable from the figure below (Figure 9.3), the behavior captured by the sensing device is the one expected, because the device was designed in order to have a resonant frequency of around 600 Hz. Indeed, in a 5 ms division, there are three periods, and furthermore the damping effect is also clearly visible as it attenuates the oscillations over time with a negative exponential characteristic. In conclusion, the system is capable, as expected, to analyze the resonant behaviour of, for instance, a beam.

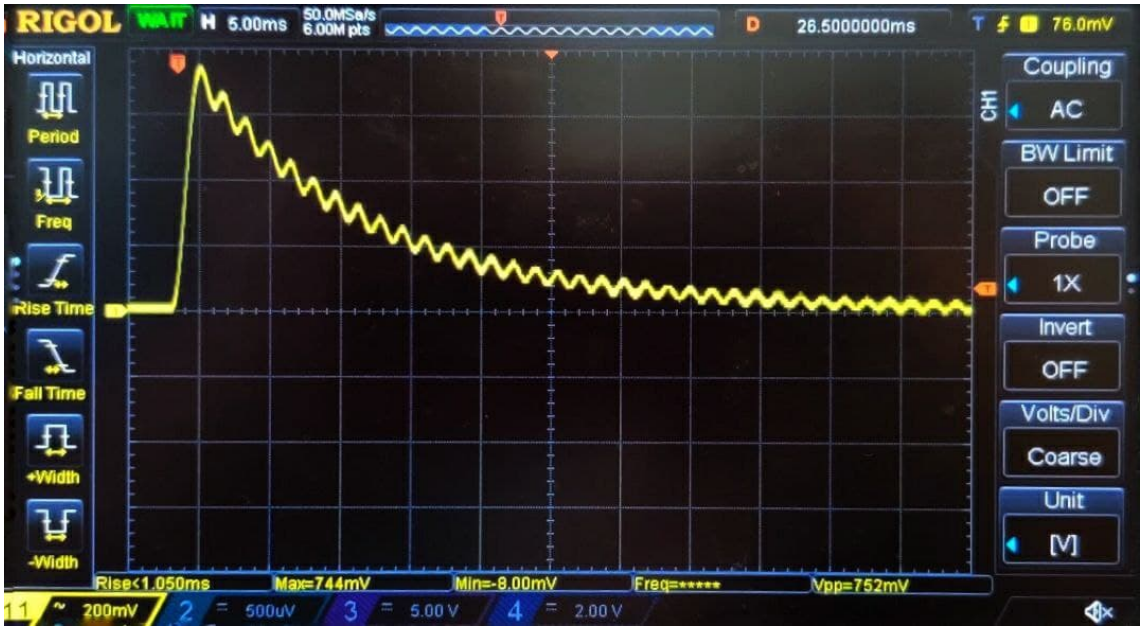


**Figure 9.3:** Time-domain response of the mass-spring-damper system

As a final example test, the main idea is to show how this measurement system is able to evaluate the presence and the approach of a person. As can be seen from the following plot (Figure 9.4), each peak corresponds to a step of one of the authors, who at the beginning is far away and at each step progressively approaches the sensor, and then moves away again. The intensity obviously varies according to the proximity of the person to the measurement system, in fact, as it can be seen, the system is roughly symmetrical.

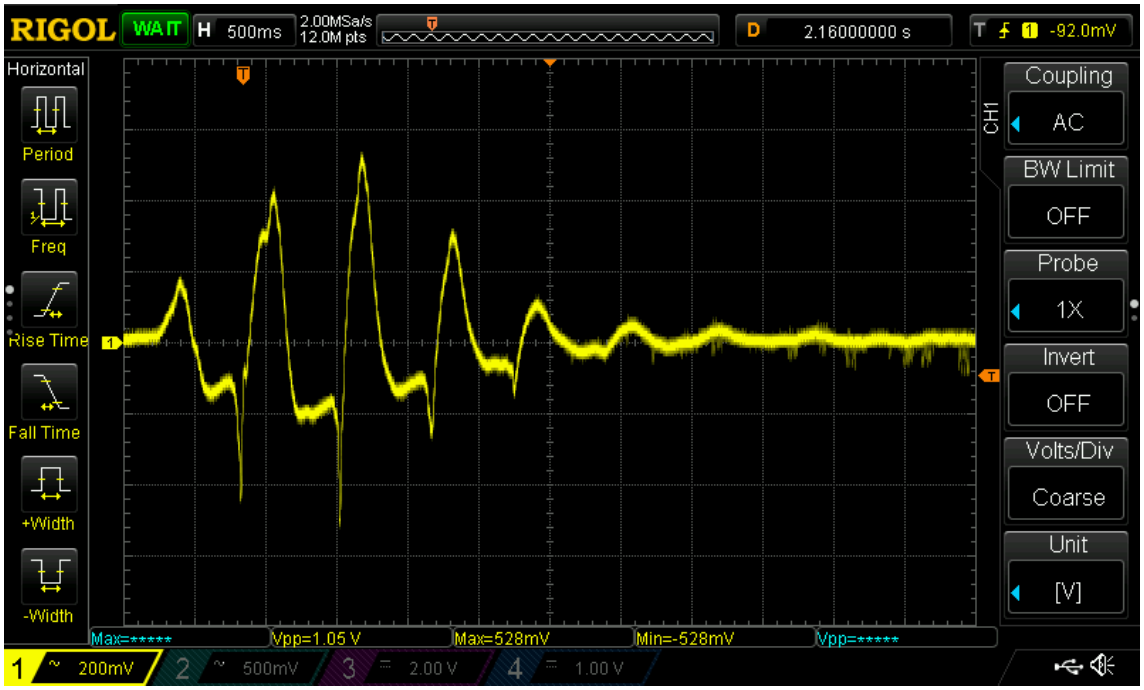


**Figure 9.4:** A person walking next to the sensor

Specifically, 8 steps are observed from the graph, the third represents the moment in which the person is closest to the sensor. Moving far away the intensity becomes smaller.

## 9.2 Systems comparison

The aim of this section is to compare the two systems, as will be appreciable later on, they behave in the same exact way, with the exception of the fact that, basing on how the sensor has been designed, the Bragg grating has been glued in the upper part, opposite to the face reserved for the plastic optical fibers. In this way, when the FBG detects a contraction, the POF sensor will sense an expansion, and vice versa. This implies having the two signals of opposite sign, but with the same behavior.

What has just said, is appreciable in the figure below (Figure 9.5), which shows the acquired signal, generated by a relatively weak punch on the table jointly liable with the sensor system.

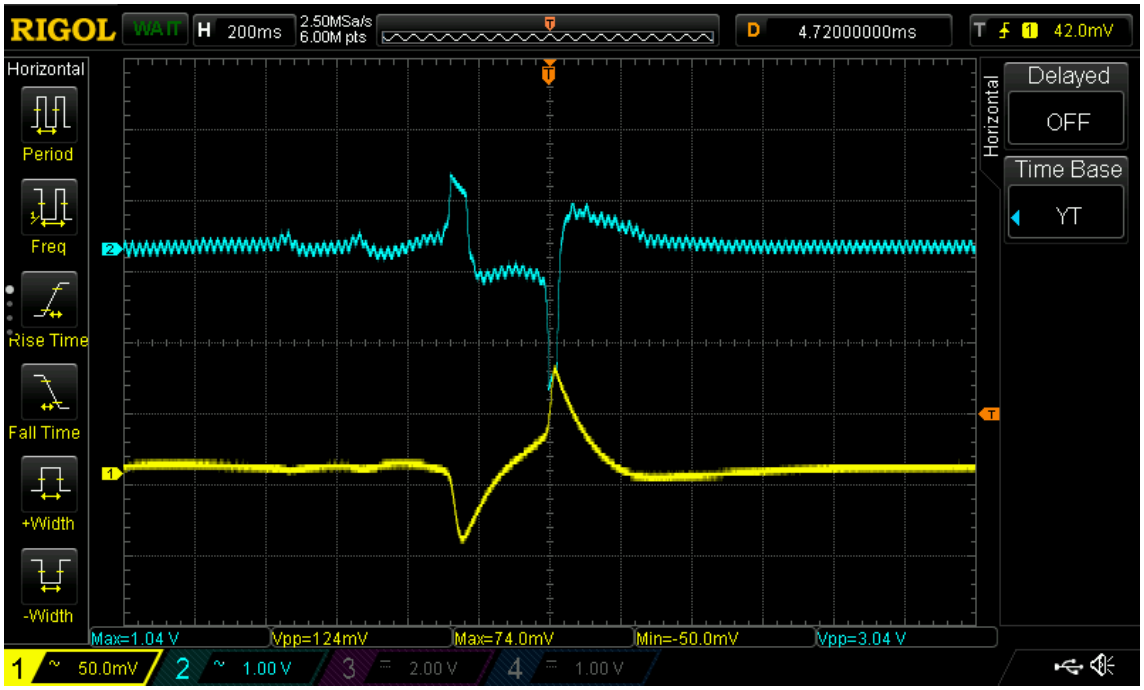


**Figure 9.5:** Opposite polarity behavior between the two systems

A further modification applied to the two system, is regarding the time constant, in order to demonstrate that they behave in a different way.

For this reason, the image proposed (Figure 9.6), wants to show this peculiarity. In fact, as can be noticed from the scope, the response times of the circuit that uses the plastic fibers (the second channel, represented in blue) are clearly smaller (about 10 times), in fact, as the project is developed, it was designed to have two different behaviors over time.

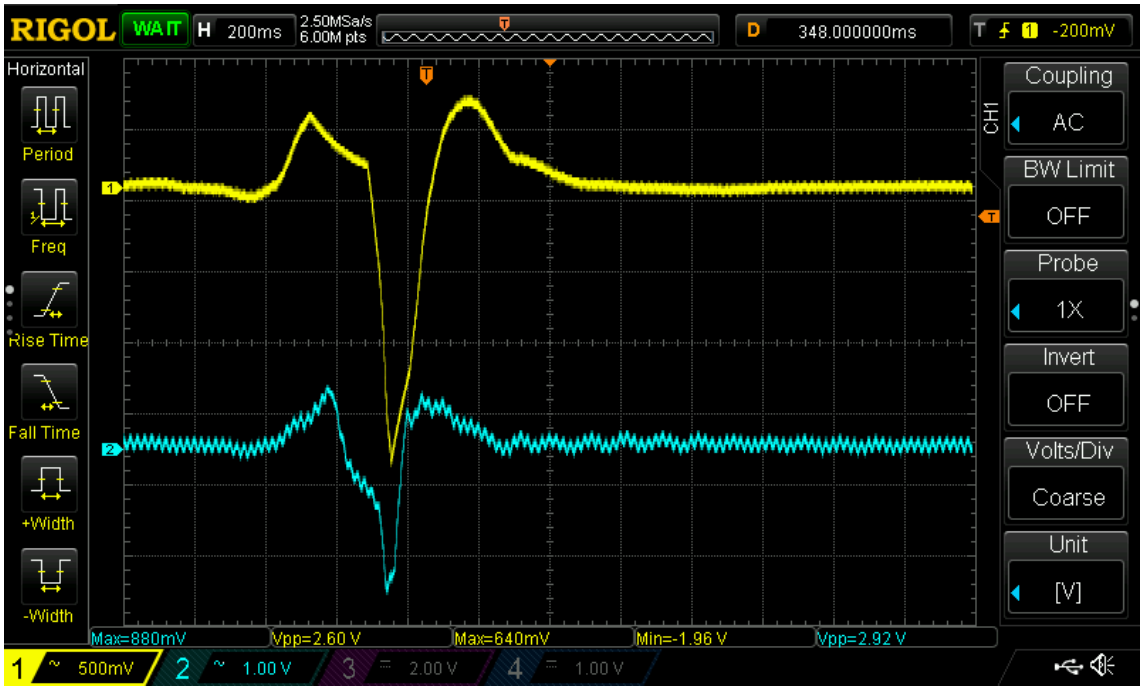


**Figure 9.6:** Different time constant demonstration

This image was obtained by adding an inverter amplifier to only one of the systems (the one that uses the POFs), with the aim to obtain a response with concordant ascents and descents, in order to better appreciate the transient response.

The last image (Figure 9.7) represents a signal generated by the repeated hopping on a spot next to the sensor (about 1 m away) by one of the authors. In this image is again appreciable the different time constants effect. Furthermore, this time, instead of adding an inverting amplifier to one of the two arrangements, an inverting stage has been removed, leading to a great peak-to-peak voltage difference in terms of amplitude.

This graph represents also very well the correct functioning of the system inside its flat band frequency range: the hopping period is roughly 400 ms as appreciable from the oscilloscope, so the frequency is of 2.5 Hz, that falls inside the 0.13 Hz to 15 Hz pass band.

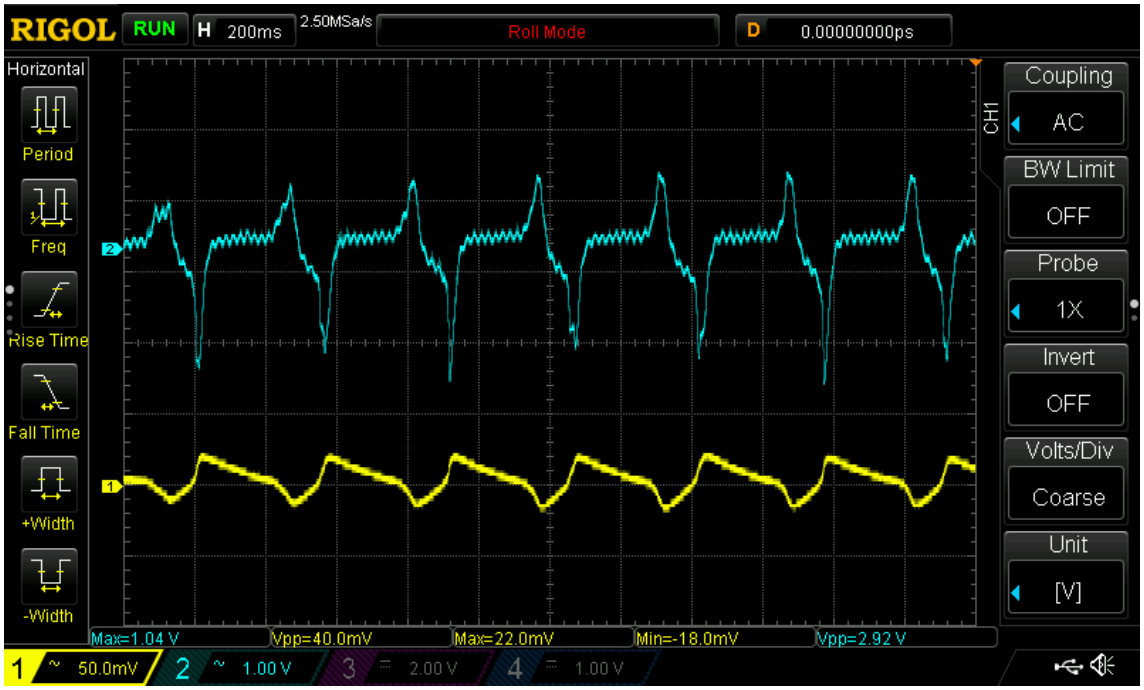


**Figure 9.7:** Repeated hopping on a spot next to the sensor

## 9.3 Shaker test

As a further and concluding test, the sensor was fixed in a jointly liable way on the EST240, a professional and programmable shaker. This simulation took place to verify if the system was able to work also outside the bandwidth of the analog circuit frequency response. For this reason, a sweep of vibrations has been set starting from 20 Hz until reaching 200 Hz, with an intensity equal to 2g. Graphically, recalling the bode diagram presented during the LT Spice simulation in the analog circuit chapter, it is appreciable in Figure 9.8 where the measurement points are placed.

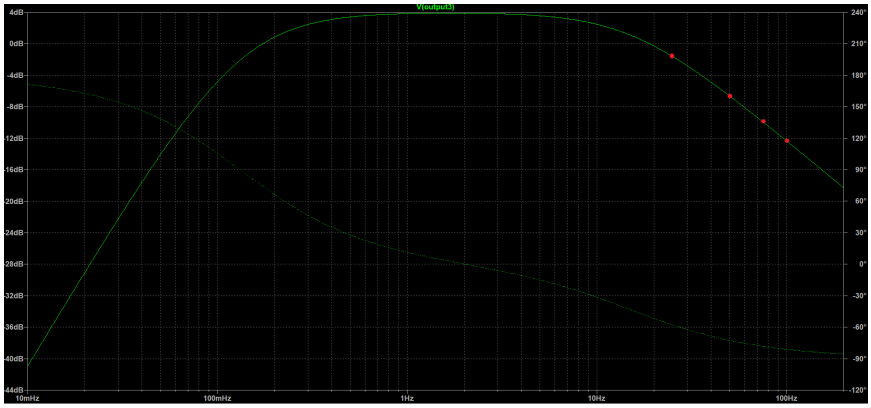

**Figure 9.8:** Shaker vibrating at 25 Hz response

The waveform captured by the vibration system should be sinusoidal, because the shaker swings the system forward, with positive acceleration, stops it, and then resumes in the opposite direction, with negative and constant acceleration. The results obtained (shown in the figures below, from Figure 9.9 to Figure 9.11), are surprising: they exactly follow the desired results.

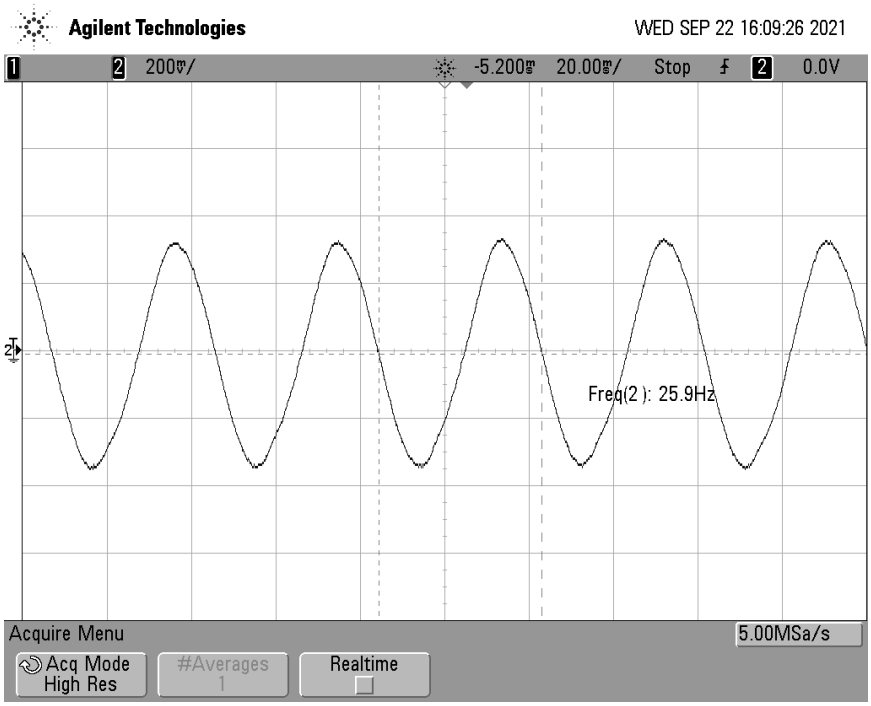


**Figure 9.9:** Shaker working points on the bode plot

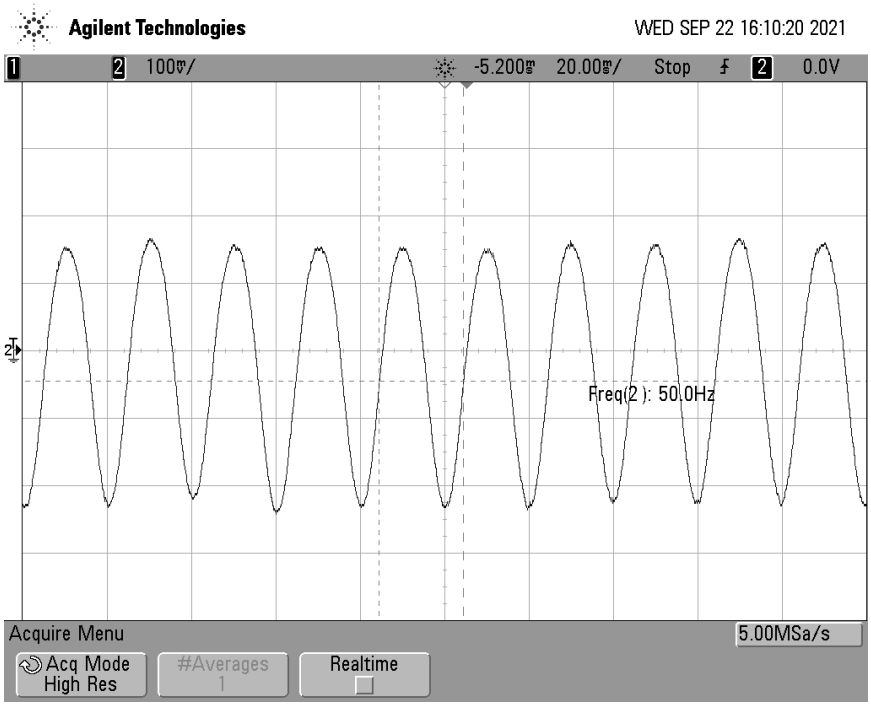


**Figure 9.10:** Shaker vibrating at 50 Hz response

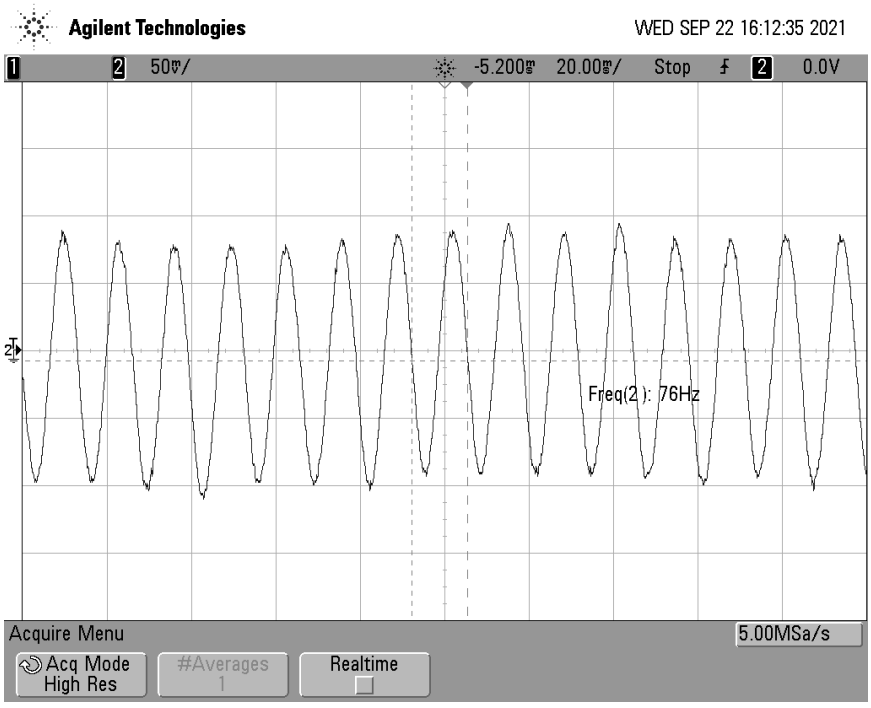


**Figure 9.11:** Shaker vibrating at 75 Hz response

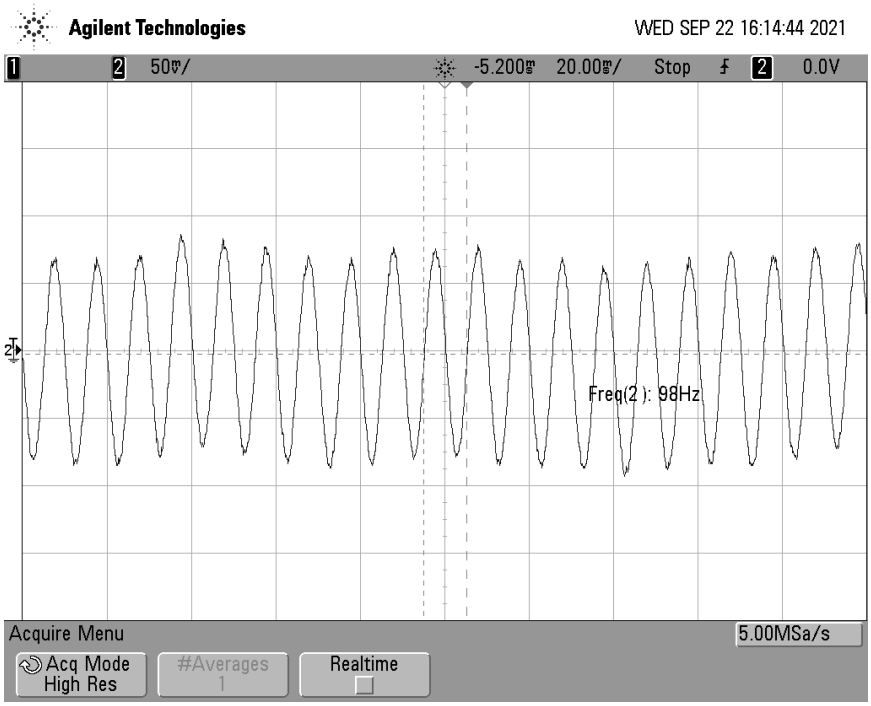


**Figure 9.12:** Shaker vibrating at 100 Hz response

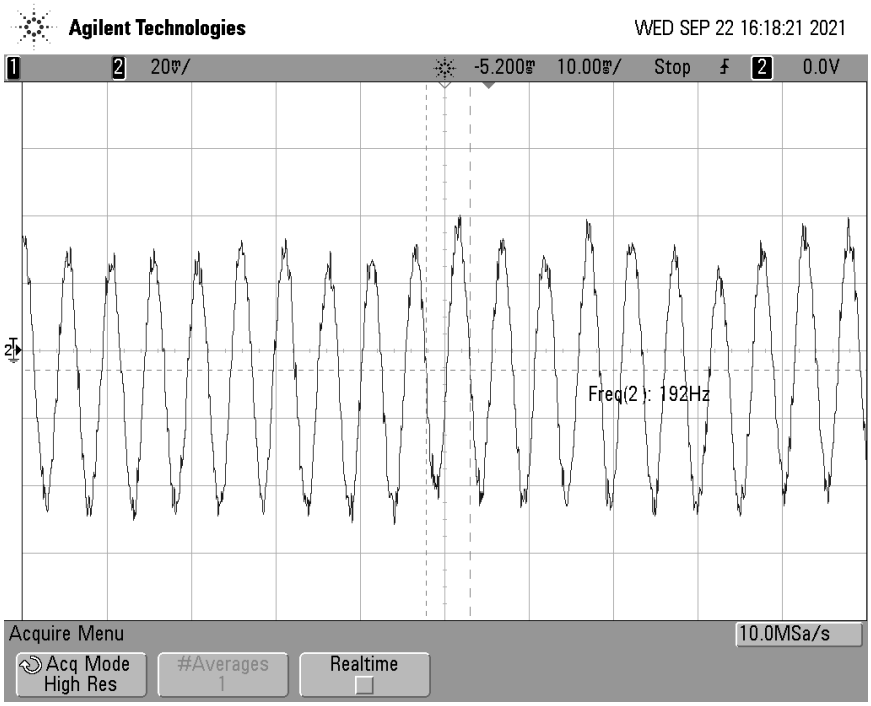


**Figure 9.13:** Shaker vibrating at 200 Hz response

The graph shows that the system is able to track the incoming signal very well: the measured frequencies (those shown on the oscilloscope screen) are well close to those provided as input to the sensor. Certainly, as the frequency increases, the device faces more difficulties to detect exactly the stimulus, but, following the data provided by the images, @200 Hz the error is given as equation 9.1.

$$e = \frac{200\,\text{Hz} - 192\,\text{Hz}}{200\,\text{Hz}} = 0.04 = 4\% \tag{9.1}$$

Another feature from the graphs above is that, having chosen frequencies of vibration outside the band, the fact of seeing the amplitude of the oscillations decrease progressively is qualitatively correct, as the bode plot of the magnitude suggests. For a quantitative evaluation of the test correctness, we can take into account Figure 9.9 and Figure 9.13, which represent the response respectively at 25 Hz and 200 hertz, meaning that, there is almost a distance of a decade on the logarithmic axis of the bode diagram. Comparing the amplitudes of the two sinusoids in the images considered, it is appreciable that the first has an amplitude of almost 4 divisions with a vertical scale of 200 mv / div, therefore $V_{\text{pp}} \cong 700\,\text{mV}$; the second, on the other hand, occupies 4 divisions with a vertical scale of 20 mv / div, therefore $V_{\text{pp}} \cong 80\,\text{mV}$. From these data it is possible to confirm that the experimental result conforms to the theory, as a decade with a slope of -20 dB/dec is reported on linear axes as dividing by a factor of 10. To be precise, the scale factor is 8.75 instead of 10: this is due to the fact of not having measured the signal at a distance of exactly one decade, but a little less.

# Chapter 10

# Conclusions

The starting point of this study was to design and develop a fiber optic based sensing system for dynamic displacement and vibration monitoring, considering two different sensors, using different technologies. The first one, more sophisticated, exploiting two matched Bragg gratings, while the second one is rawer and is based on facing plastic optic fibers, but on the contrary is more sensitive.

The principle of operation provides that the information is coded into a light signal in an intensiometric way to avoid the use of more expensive and complicated detectors: in both applications the input of the electronic circuit is just a current generated by two different photodiodes.

As expected, the FBG based sensor gave better performances in terms of noise and disturbances rejection and, furthermore, it is not sensitive to external light sources coming from the environment, because the photo-detector is fiber coupled. The second arrangement, instead, is more sensitive, leading to less amplification issues, but, in order to work properly, it has to be encapsulated in a dark case to avoid perturbations from the environment light. Summing up, the facing fibers technology made fewer design issues arise, but, as already known from the literature, they are not able to maintain the same behavior over time, as, instead, FBG based systems are.

Since both systems are based on a light intensity conversion into a current quantity through a photo-diode, the conditioning circuit can be developed once for all: the amplifying circuit is the same with the only difference of the value of some resistors and capacitors. Moreover, the electronic circuit has been closed in a Faraday's cage that screens all the electromagnetic interference coming from the main power.

It is appreciable how the two systems can sense the same kind of vibrations, but their utilization ambit and environment application are quite different due to the fact that their cost are completely unlike. For example, the FBG based setup is preferred to be used in an application in which very good reliability and several sensors are required, as the monitoring of a bridge resonating frequency to check for its structural stability. Having several sensor heads, it is possible to use in a clever

way the expensive single mode wide spectrum light source: this is done by means of an AWG (Arrayed Waveguide Grating) that is capable to split the source large spectrum into several fibers with narrow band. The drawback is that, unfortunately, each of these channels require a photodetector and its own conditioning circuit, so the arrangement is still not completely optimized, but this can be a further improvement for future researches.

On the contrary, the POF based arrangement is more suitable for what concerns simple sensing systems, since it is very cheap and its hardware failures are easy to be managed. Furthermore, this kind of setup is particularly convenient in harsh and rough environments, because their configuration made of sensor, fiber, circuit and radio module can be entirely powered by a battery pack and placed in the hostile environment. The optimization of the batteries, alongside with the research about the plastic fiber lifetime before the performance degradation, can be, again, argument of future studies.

Moreover, a link to the PC has been established by means of serial or radio communication, alongside with a Python acquisition program, in order to collect data on a powerful computer. This trick allows to manipulate raw data, without the need of interrupting the sensing operations during the processing.

Inside this the software field just mentioned, several further improvement can be applied on the whole system: for example, to improve the program algorithm capabilities by implementing some functions, as peak envelope detector, FFT and the possibility to collect and process data coming from different sensing systems. Another feature that can be developed is to acquire data also in single mode and save all samples. Applications of this kind of functions are spread and useful, as, for instance, the FFT implementation can be exploited to analyse beams' structural health, studying its resonant frequency components.

For this thesis both optical circuits have been entirely simulated, designed and assembled, the PCBs have been designed and manufactured using a CAD/CAM software. For prototyping it has been necessary to mill a PCB using a CNC machine, because it is more robust than a circuit on a breadboard and it will avoid some disturbances and parasitic capacitance. Furthermore, the microcontroller has been programmed to sample the input signal and the protocols to connect with the PC via serial and radio communication have been arranged, alongside with Python software for the live plot of the sampled data. As a last consideration, the system has been created and tested, confirming its functioning.


**Figure 10.1:** The sensor

# Appendix A

# Python software

```
import os
import numpy as np
import multiprocessing as mp
import matplotlib.pyplot as plt
import time
import serial

global packet_length
packet_length = 500
global working_period
working_period = 40

def live_plotter(x_vec,y1_data,line1,identifier='',pause_time=0.1):
    if line1==[]:
        # this is the call to matplotlib that allows dynamic plotting
        plt.ion()
        fig = plt.figure(figsize=(13,6))
        ax = fig.add_subplot(111)
        # create a variable for the line so we can later update it
        line1, = ax.plot(x_vec,y1_data,'-o',alpha=0.8)
        #update plot label/title
        plt.ylabel('Y Label')
        plt.title('Title: {}'.format(identifier))
        plt.show()
    # after the figure, axis, and line are created, we only need to
    update the y-data
    line1.set_ydata(y1_data)
    # adjust limits if new data goes beyond bounds
    if np.min(y1_data)<=line1.axes.get_ylim()[0] or np.max(y1_data)>=
    line1.axes.get_ylim()[1]:
        plt.ylim([np.min(y1_data)-np.std(y1_data),np.max(y1_data)+np.
    std(y1_data)])
```

```
30      # this pauses the data so the figure/axis can catch up - the amount
        of pause can be altered above
31      # if pause_time != 0:
32      plt.pause(pause_time)
33
34      # return line so we can update it again in the next iteration
35      return line1
36
37  def put_value(q,end_signal):
38      ser = serial.Serial('COM7', 500000)
39      ser.flush()
40      ser.flushInput()
41      ser.flushOutput()
42      data_packet = []
43      t0 = time.time()
44      times = []
45
46      while end_signal.value == 0:
47          if ser.in_waiting != 0:
48              read = ser.read(2)
49              if ((read[0] + 256*read[1]) > 1023):
50                  ser.read(1)
51              else:
52                  data_packet.append(read[0]+256*read[1])
53                  if len(data_packet) == packet_length:
54                      q.put(data_packet,block = False)
55                      data_packet = []
56                      times.append(time.time()-t0)
57                      t0 = time.time()
58      ser.close()
59      print('process put_value done')
60
61  #MAIN LOOP
62  if __name__ == '__main__':
63      plt.style.use('ggplot')
64      line1 = []
65      x_vec = np.arange(1,packet_length + 1)
66      times = []
67      counter = 0
68      end_signal = mp.Value('i', 0)
69      q = mp.Queue()
70      p1 = mp.Process(target = put_value, args = (q,end_signal))
71      p1.start()
72      done = False
73      t0 = time.time()
74
75      while done == False:
76          if time.time() - t0 > working_period:
77              done = True
78          else:
79              if q.empty() == False:
```

```
80                  counter = counter + 1
81                  t1 = time.time()
82                  new_data = q.get(timeout = 100e-3)
83                  times.append(time.time()-t1)
84                  line1 = live_plotter(x_vec,np.array(new_data),line1,
    pause_time= 0.05)
85      plt.close()
86      end_signal.value = 1
87      p1.join()
```

$\mathcal{O}(n \log n)$

`numpy`

# Bibliography


[1] G. Perrone D. Tosi and A. Vallan. «Performance Analysis of a Noncontact Plastic Fiber Optical Fiber Displacement Sensor with Compensation of Target Reflectivity». In: 2013 (2013), pp. 4–8 (cit. on pp. 6, 8).

[2] H. Z. Yang X. G. Qiao D. Luo K. S. Lim W. Chong and S. W. Harun. «A review of recent developed and applications of plastic fiber optic displacement sensors». In: 36 (2013), pp. 3–6 (cit. on p. 7).

[3] H. Cao, Y. Chen, Z. Zhou, and G. Zhang. «Theoretical and experimental study on the optical fiber bundle displacement sensors». In: 36 (2007), pp. 5–7 (cit. on pp. 7, 8).

[4] *si155 HYPERION Optical Sensing Instrument data sheet*. Atlanta, United States: Micron Optics (cit. on pp. 17, 18).

[5] *I-MON USB Interrogation Monitors data sheet*. Ryttermarken, Denmark: Ibsen Photonics (cit. on p. 18).

[6] *FIBER OPTICAL ACCELEROMETER*. Neuchâtel, Svizzera: Sercalo Microtechnology (cit. on p. 18).

[7] J.B. Faria. «A Theoretical Analysis of the Bifurcated Fiber Bundle Displacement Sensor». In: 47 (1998), pp. 2–6 (cit. on pp. 19, 22).

[8] *LMx24-N, LM2902-N Low-Power, Quad-Operational Amplifiers data sheet*. Dallas, United States: Texas Instruments (cit. on p. 44).